An experimental investigation of symmetric and asymmetric turbulent wake development in pressure gradient

Flint O. Thomas and Xiaofeng Liu
Center for Flow Physics and Control, The University of Notre Dame, Notre Dame, Indiana 46556

(Received 4 June 2003; accepted 23 January 2004; published online 8 April 2004)

This paper examines and contrasts the response of planar turbulent wakes with initially symmetric and asymmetric mean velocity profiles to identical imposed streamwise pressure gradients. The focus on near wake behavior, profile asymmetry, and pressure gradient is motivated by their relevance to high-lift systems for commercial transport aircraft. In the experiments, the symmetric wake is generated by a flat plate with a tapered trailing edge. Active and passive flow control are applied on an identical second plate in order to generate the asymmetric wake. Both favorable and adverse *constant* pressure gradients are imposed on the wakes by means of a downstream diffuser section with fully adjustable top and bottom wall contour. For both symmetric and asymmetric wakes, the effect of pressure gradient on wake spreading, mean velocity defect decay, and the streamwise evolution of the turbulent stresses are documented in detail. In this manner, the role of asymmetry in strained wake development is isolated. We also gauge the ability of commonly used one- and two-equation turbulence models to predict the streamwise wake evolution observed in the experiments. [DOI: 10.1063/1.1687410]

I. INTRODUCTION

In multielement airfoils used for high-lift in transport aircraft, the wake from an upstream element develops in a strong pressure gradient environment imposed by downstream elements. The effect of the pressure gradient on global wake development will have a profound effect on the aerodynamic performance of the high-lift system. For example, the rate of slat wake spreading will influence the degree of confluence with the main element or flap boundary layers. Even in the absence of confluence, the wake spreading will effect the degree of pressure peak moderation on the trailing flap(s) and thereby influence flap flow attachment.[1] Smith[2] notes that off-surface flow reversal can occur if a wake encounters a sufficiently strong adverse pressure gradient. Several recent studies have exposed turbulent wakes to adverse pressure gradients of sufficient strength to cause reversed wake flow.[3–6]

The turbulent wake in pressure gradient has also received considerable attention as an example of a canonical free turbulent shear flow exposed to streamwise straining. However, the focus of most work has been on the asymptotic response of symmetric turbulent wakes to spatially varying pressure gradients or the relaxation process by which an equilibrium wake responds to localized impulse-like pressure perturbations (e.g., Refs. 7–13).

In marked contrast to these studies, Liu[14] and Liu *et al.*[15] investigated the symmetric, planar turbulent near-wake exposed to *constant* favorable and adverse streamwise pressure gradients. The focus on the near wake was motivated by its relevance to high-lift aerodynamics. It was demonstrated that the mean flow and turbulence quantities in the wake are extremely sensitive to the applied pressure gradient. For example, even a modest adverse pressure gradient was found to have a profound effect on the mean flow spreading and velocity defect decay rate. Along with the enhanced wake widening, the adverse pressure gradient condition was found to yield higher levels of turbulent kinetic energy than in the zero pressure gradient wake. In contrast, the favorable pressure gradient case exhibited a reduced spreading rate, increased defect decay rate, and a more rapid decay of turbulence kinetic energy relative to the zero pressure gradient case. Using a similarity analysis, explicit relations for the streamwise variation of global mean flow parameters were derived that capture the essential features of the wake's response to imposed pressure gradients.

Due to the disparate shear layer development that occurs over the top and bottom surfaces of a high-lift system leading edge slat, the wake mean velocity profile tends to be inherently asymmetrical in shape.[16] It is important, therefore, to also characterize the response of asymmetric turbulent wakes to imposed pressure gradients. Previous studies have examined the asymmetric wakes that result from the disparate top and bottom surface boundary layer development that occurs on airfoils at angle of attack (e.g., Hah and Lakshminarayana[17] and Acharya, Adair, and Whitelaw[18]). However, in these studies the wake development occurred in a nominally zero pressure gradient environment. A notable exception is a fundamental study by Roos[19] that was also motivated by high-lift applications. Roos[19] used passive flow control of the boundary layer on a splitter plate in order to generate an initially asymmetric wake profile which was then exposed to a strong adverse pressure gradient generated by a pair of airfoils.

II. OBJECTIVES

This paper will examine and contrast the response of initially symmetric and asymmetric planar turbulent near

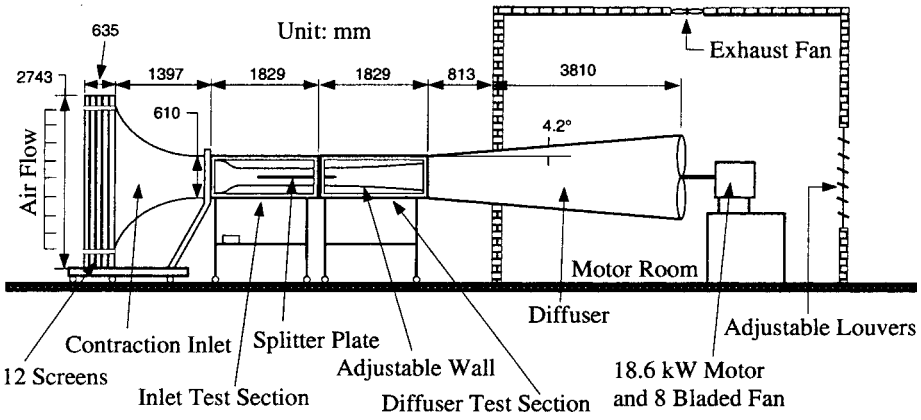

FIG. 1. Schematic of the experimental facility.

wakes to identical imposed *constant* favorable and adverse streamwise pressure gradients. The focus on near wake behavior, profile asymmetry, and pressure gradient is motivated by their relevance to high-lift applications. For both symmetric and asymmetric wakes, we document the effect of pressure gradient on wake widening, velocity defect decay, and the streamwise evolution of turbulent stresses. This extends the work of Liu *et al.*[15] by isolating the effect of profile asymmetry on the development of the wake. Since the ability to predict asymmetric near-wake development in arbitrary pressure gradient environments is prerequisite to achieving reliable computational fluid dynamics (CFD) design tools for high-lift systems, we also seek to gauge the ability of commonly used one- and two-equation turbulence models to predict the streamwise wake evolution observed in the experiments.

III. EXPERIMENTAL FACILITY AND MEASUREMENT APPARATUS

A. Flow field facility and model geometry

The experiments were performed in an open-return subsonic wind tunnel facility located at the Center for Flow Physics and Control at the University of Notre Dame. A schematic of the wind tunnel facility is shown in Fig. 1. This facility has been documented in detail in Liu[14] and Liu *et al.*[15] and only essential aspects will be described here.

Ambient laboratory air is drawn into a 2.74 m by 2.74 m tunnel inlet with a contraction ratio of 20.25:1. The inlet contains 12 turbulence reduction screens that yield a very uniform test section velocity profile with a free stream fluctuation intensity level that is less than 0.1% (and less than 0.06% for frequencies greater than 10 Hz).

For these experiments, the wind tunnel utilizes two consecutive test sections. The upstream test section contains a wake-generating plate while the second forms a diffuser section as shown in Fig. 1. The wake measurements were conducted in the downstream diffuser test section which is used to produce the desired adverse/favorable pressure gradient environment for wake development. The top and bottom walls of the diffuser are made of sheet metal and their streamwise contour is fully adjustable by means of seven groups of turnbuckles in order to create the desired constant streamwise pressure gradient environment. To facilitate flow visualization and laser Doppler velocimetry measurement, both test sections have one sidewall made of plate glass.

For the symmetric wake experiments, the wake generating body is a Plexiglass plate with a chord length of 1.22 m and a thickness of 17.5 mm. The splitter plate model is sidewall mounted in the test section with end plates used to minimize the influence of tunnel sidewall boundary layers. The leading edge consists of a circular arc with distributed roughness which gives rise to turbulent boundary layer development over the top and bottom surfaces of the plate. The last 0.2 m of the plate consists of a 2.2° linear symmetric taper down to a trailing edge of 1.6 mm thickness.

In order to create a wake with a skewed initial velocity distribution, both passive and active flow control was applied to a second, identical wake-generating plate as shown in Fig. 2. First, a suction slot was placed on the top surface of the

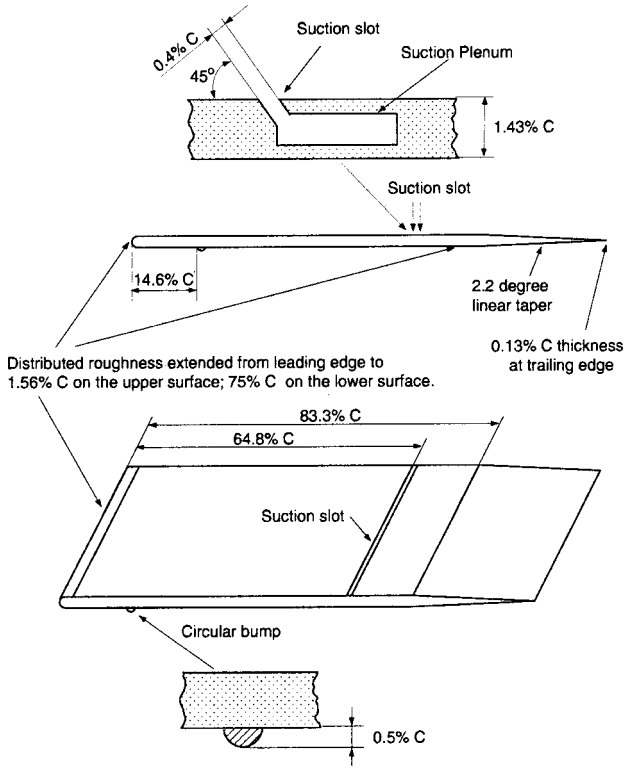

FIG. 2. Splitter plate for generation of the asymmetric wake.

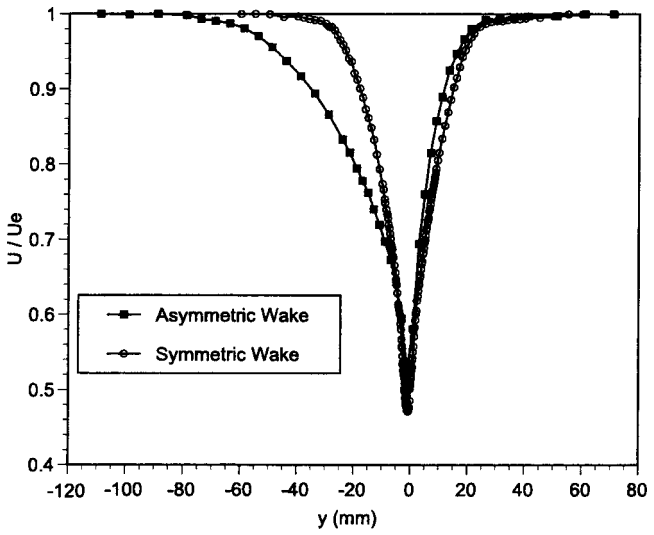

FIG. 3. Comparison of symmetric and asymmetric initial wake velocity profiles.

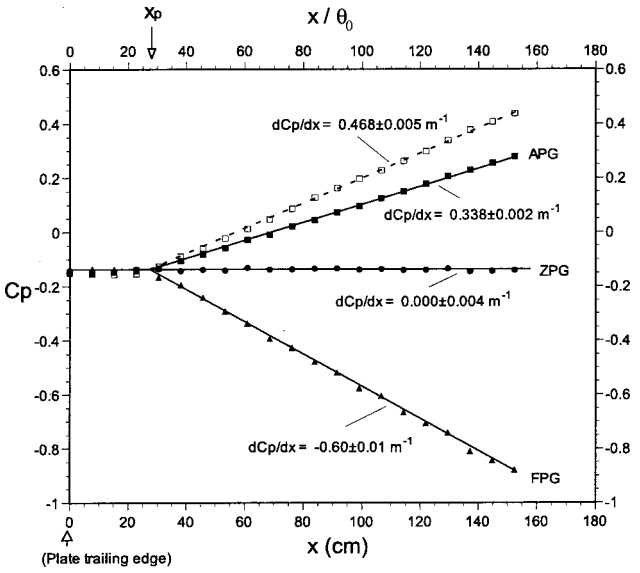

FIG. 4. Measured streamwise pressure distributions.

plate at the 65% chord position. The suction slot was connected to an internal plenum that, in turn, was connected via suitable external plumbing to a large rotary vacuum pump. Care was taken to insure that the internal plenum was baffled in such a manner as to yield a spanwise uniform suction flow at the slot. The suction slot served to thin the boundary layer on the upper surface of the splitter plate. In addition, a small semicircular, spanwise uniform bump was placed on the lower surface of the plate at the 14.6% chord location. Distributed roughness (in the form of grit tape) was placed on the lower plate surface extending from the leading edge of the plate to the 75% chord location. The combination of the bump and distributed roughness gave rise to a significant thickening of the boundary layer on the lower plate surface without incurring unsteady effects associated with the separation bubble aft of the bump. The combination of these techniques gave rise to an initially asymmetric wake profile similar to that encountered in actual high-lift systems. The degree of mean velocity asymmetry of the initial wake profile expressed as a ratio of the momentum thickness of the lower (thick) wake shear layer θ_1 to that on the upper (thin) shear layer θ_2 is $\theta_1/\theta_2=2.5$. Figure 3 compares initial wake mean velocity profiles for the symmetric and asymmetric wake cases as measured just $x=19\,\mathrm{mm}$ downstream of the plate trailing edge. The effect of the flow control in skewing the initial wake profile is apparent. As in the slat wake, it is the disparate shear layer development over the top and bottom surfaces of the plate that gives rise to the initial wake asymmetry. For additional details regarding the wake generating body and flow field facility the reader is referred to Liu.[14]

B. Imposed pressure gradients

The streamwise pressure distribution was measured by means of a series of static pressure taps located on one flat sidewall of the diffuser test section at the same lateral (i.e., y) location as the centerline of the symmetric wake. Laser Doppler velocimetry (LDV) measurements of the centerspan streamwise distribution of mean velocity in the potential flow region, $U_e(x)$, were found to be fully consistent with the measured wall pressure variation, thereby confirming the suitability of the pressure tap placement and use in the characterization of the stream-wise pressure gradient imposed on the wake. In this paper the imposed pressure will be expressed in terms of a pressure coefficient, $C_p=[P(x)-P_\infty]/q_\infty$, where $P(x)$ is the local static pressure in the diffuser, and P_∞ and q_∞ are the static and dynamic pressures, respectively, upstream of the splitter plate.

Three sets of experiments were conducted: (1) a zero pressure gradient (ZPG) base flow condition, $dCp/dx=0.0\,\mathrm{m}^{-1}$; (2) a constant adverse pressure gradient (APG) condition with $dCp/dx=0.338\,\mathrm{m}^{-1}$; and (3) a constant favorable pressure gradient (FPG) condition with $dCp/dx=-0.60\,\mathrm{m}^{-1}$. The zero pressure gradient wake served as an essential baseline case for comparison with the nonzero pressure gradient-wake development. In each case, a common zero pressure gradient zone occurs immediately downstream of the splitter plate trailing edge in order to ensure that the wake initial condition is identical in each case.

The measured streamwise pressure distributions corresponding to these different experimental conditions are shown in Fig. 4. As indicated, the pressure gradients are initially applied downstream of the plate trailing edge at a common location designated x_p. Also shown in this figure is a larger adverse pressure gradient case that was run but found to give rise to intermittent, unsteady flow separation near the aft portion of the diffuser wall. Wake measurements for this case will not be presented. This case may be regarded as an effective upper limit on the magnitude of the constant adverse pressure gradient that can be produced by the diffuser without incurring intermittent, unsteady flow separation effects.

Before conducting the detailed flow field surveys for the different pressure gradient cases, the quality of the flow field in the diffuser test section was carefully examined. These

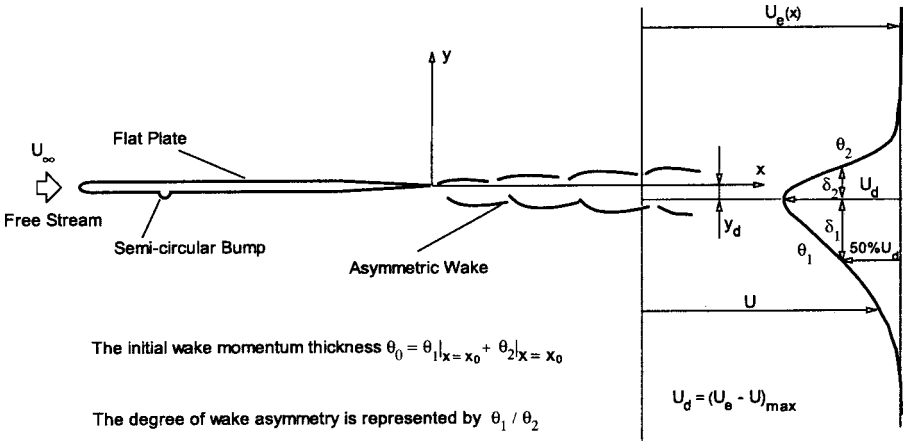

FIG. 5. Wake mean flow development nomenclature.

measurements verified the two-dimensionality of the flow field in the mean. In particular, profiles of mean velocity and turbulence quantities at fixed x for several spanwise locations across the test section exhibited nearly perfect collapse. These measurements indicate that the mean flow remains spanwise uniform in the diffuser test section up to the last measurement station at $x=1.52$ m.

C. Flow field parameters

The experiments were performed at a Reynolds number of $\mathrm{Re}=2.4\times10^6$ (based on the chord length of the splitter plate and a free stream velocity of $U_\infty=30$ m/s) for all cases. It may be noted that during landing approach, a Boeing 737-100 will have a Reynolds number based on slat chord of about 1.8×10^6, a value quite comparable to this experiment.

For ZPG, APG, and FPG cases involving the symmetric wake, the initial wake momentum thickness $\theta_0=7.2$ mm and the Reynolds number (based on initial wake momentum thickness) $\mathrm{Re}_\theta=1.5\times10^4$. For the asymmetric wake the initial momentum thicknesses of the lower and upper shear layers are $\theta_1=7.13$ mm and $\theta_2=2.88$ mm, respectively ($\theta_1/\theta_2=2.5$). The initial momentum thickness of the asymmetric wake is $\theta_0=\theta_1+\theta_2=10$ mm and the corresponding $\mathrm{Re}_\theta=2.1\times10^4$.

D. Flow field diagnostics

The streamwise development of the symmetric and asymmetric wake mean and turbulent velocity field for the selected pressure gradients was investigated nonintrusively with an Aerometrics three-component fiber optic LDV system and also with constant temperature hot-wire anemometry. Wherever possible, both techniques were employed in order to insure the fidelity of the data.

The fiber-optic LDV system was typically operated in two-component back-scatter mode with 514.5 and 488 nm laser wavelengths used to measure the streamwise, u, and cross-stream, v, components of velocity, respectively. Frequency shifting was used in order to unambiguously resolve flow direction. The measurements were made in the coincidence mode and results for both mean flow and turbulence quantities presented in this paper represent ensemble averages over at least 10 000 valid coincident LDV burst events. Wind tunnel seeding was performed at the tunnel inlet with an Aerometrics particle generator model APG-100 using a 1:2 mixture of propylene glycol and distilled water. The transceiver of the LDV system was mounted to a computer-controlled traverse table. The accuracy of the movement of the traverse table in both the horizontal and vertical direction was 0.4 μm. The streamwise and cross-stream dimensions of the measurement probe volume of the LDV system was 234.4 and 234.0 μm, respectively.

The LDV surveys were repeated using constant temperature hot-wire anemometry. For the reported hot-wire measurements a multichannel TSI IFA 100 anemometer together with miniature x-wire probes (Auspex type AHWX-100) were used. The anemometer output was anti-alias filtered at 10 kHz and digitally sampled at 20 kHz. The total record length at each measurement station was 26.2 s which yielded fully converged turbulence statistics.

Comparison between the LDV and x-wire measurements showed excellent agreement in both mean flow and turbulence quantities with the exception of the free stream turbulence intensity levels which are overpredicted by the LDV. This is a well-known signal-to-noise ratio problem when LDV measurement systems are operated in very low-turbulence free stream environments.

IV. RESULTS

In this section measurements characterizing the streamwise evolution of both mean and turbulent flow quantities for the symmetric and asymmetric wakes are presented and compared. We first describe the mean flow development followed, in turn, by the second-order turbulence statistics.

A. Wake mean flow development

In this section experimental results are presented which document the mean flow development of symmetric and asymmetric turbulent plane wakes exposed to the same constant pressure gradients. In each case, these results are based upon cross-stream LDV and hot-wire traverses of the wake over the full range of streamwise locations in the diffuser section. Figure 5 illustrates wake mean flow nomenclature that will be used in describing the mean flow evolution of the wake. As indicated in Fig. 5, x, y, and z denote the stream-

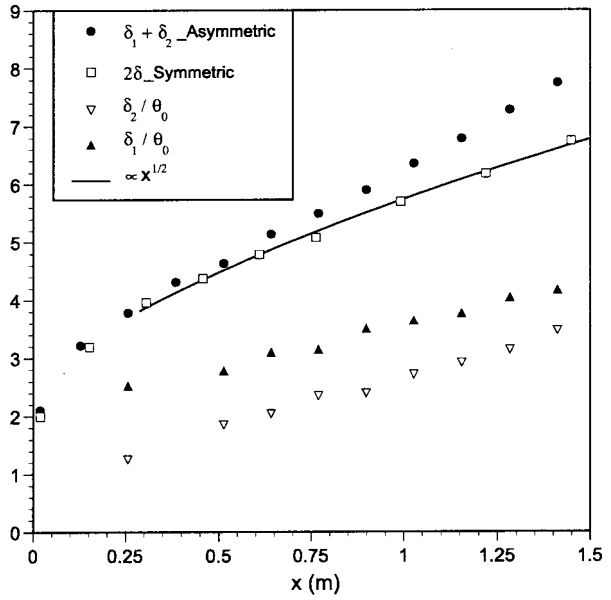

FIG. 6. Comparison of ZPG wake spreading for the symmetric and asymmetric wake cases.

wise, lateral (cross-stream), and spanwise spatial coordinates, respectively. For the asymmetric wake, the thicknesses of the two wake shear layers will not be the same and will be denoted $\delta_1(x)$ and $\delta_2(x)$ as indicated. These thicknesses are defined as the lateral distance from the location of local maximum velocity defect, $U_d \equiv [U_e(x) - U]_{\max}$, to the location where the defect drops to 50% of U_d in the thick and thin shear layers, respectively. The local asymmetric wake half-width is then defined as $\delta \equiv (\delta_1 + \delta_2)/2$. For the symmetric wake no distinction between individual wake shear layer thicknesses needs to be made since $\delta_1 = \delta_2$. In this case δ, as defined above, yields the conventional wake half-width. Since the flow control used to generate the wake asymmetry also gives rise to a disparity in initial wake thickness (between symmetric and asymmetric cases), the wake spreading will be compared in terms of a normalized wake width $\delta(x)/\theta_0$. For the symmetric wake the local maximum velocity defect U_d occurs at the centerline of the wake ($y = 0$). For the asymmetric wake the lateral location associated with U_d is denoted y_d and varies with streamwise distance x as will be demonstrated in results to be presented.

1. Asymmetric wake mean flow development in zero pressure gradient

In order to gain an initial appreciation for the effect of profile asymmetry on wake mean flow development, we first examine the baseline zero pressure gradient case. Figure 6 presents the streamwise variation of the normalized wake width $\delta(x)/\theta_0$ for both the symmetric and asymmetric zero pressure gradient cases. It is well known that the symmetric wake half-width, $\delta(x)$, and the local maximum velocity defect, $U_d(x)$, vary with streamwise distance as $x^{1/2}$ and $x^{-1/2}$, respectively, given sufficient distance downstream of the wake generating body (Schlichting[20]). Figure 6 shows that the symmetric wake width gradually approaches the expected $x^{1/2}$ variation. In contrast, the asymmetric wake

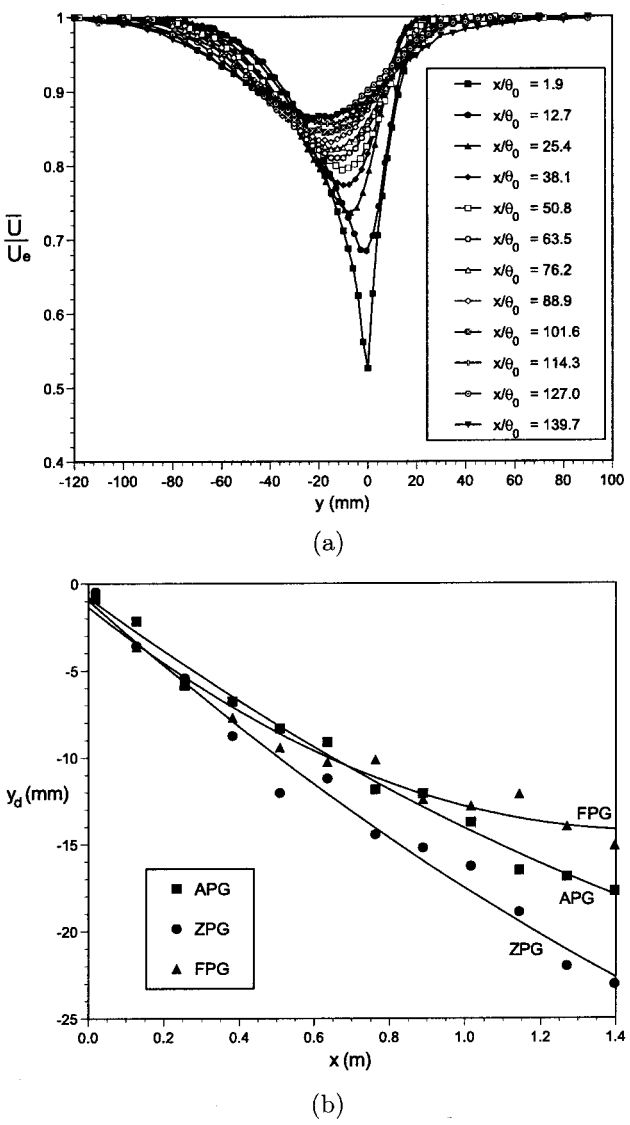

FIG. 7. (a) Asymmetric wake mean velocity profiles for the ZPG case, and (b) stream-wise variation in $y_d(x)$.

spreads at a rate that clearly exceeds that of the symmetric wake. Figure 6 also presents the streamwise growth of the individual asymmetric wake shear layers denoted $\delta_1(x)/\theta_0$ and $\delta_2(x)/\theta_0$. Note that the spreading rate of the thinner wake shear layer exceeds that of the thicker shear layer and, as a consequence, $\delta_2(x)$ gradually approaches $\delta_1(x)$ with downstream distance. This implies that the asymmetric wake mean velocity profile gradually becomes more symmetric with streamwise distance. This effect is also evident in Fig. 7(a) which shows a series of ZPG asymmetric wake mean velocity profiles measured at several representative streamwise locations. The trend toward the development of a more symmetric mean velocity profile is apparent. Another feature of the asymmetric wake mean flow development that is apparent from Fig. 7(a) is a lateral migration of the location of maximum local velocity defect with x. In particular, the lateral location of the maximum local velocity defect $y_d(x)$ is not fixed at $y = 0$, as is the case for the symmetric wake, but instead migrates toward the thicker side of the wake with

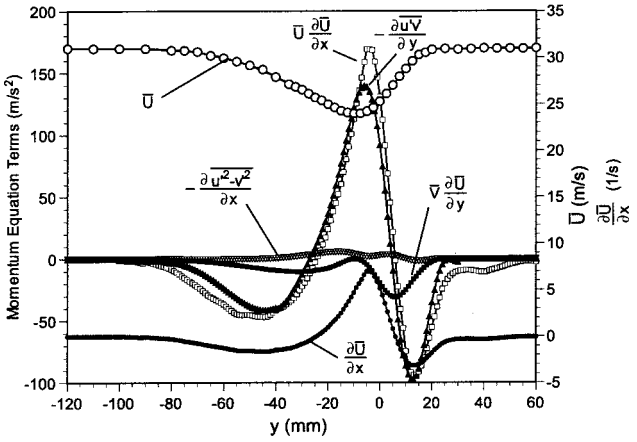

FIG. 8. Cross-stream profiles of x-momentum equation terms at $x/\theta_0 = 38.1$ for the asymmetric wake ZPG case.

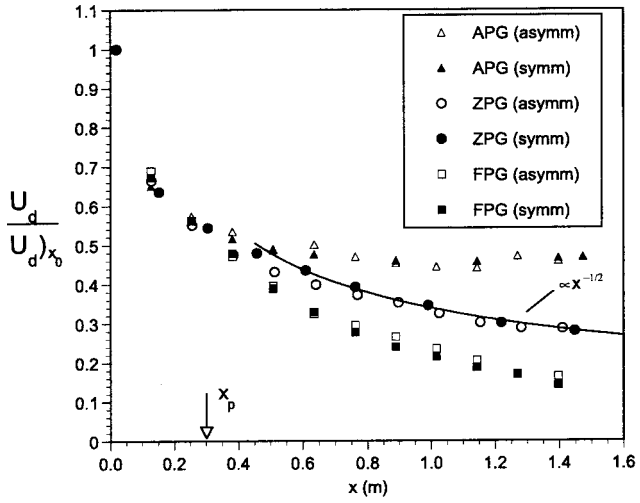

FIG. 9. Streamwise variation in maximum velocity defect for the symmetric and asymmetric wakes.

downstream distance. This effect is clearly shown in Fig. 7(b) which presents the measured streamwise variation, $y_d(x)$, for the ZPG asymmetric wake (as well as for the APG and FPG cases which exhibit a similar variation with x). This aspect of the wake development is not unique to this experiment. In fact, a similar cross-stream migration of the maximum defect location toward the thicker slat wake shear layer has been observed in a high-lift system as reported by Thomas *et al.*[16]

In order to understand the origin of the streamwise variation of $y_d(x)$, consider the streamwise momentum equation for the ZPG wake, which in the thin shear layer approximation is given by

$$\bar{U}\frac{\partial \bar{U}}{\partial x} + \bar{V}\frac{\partial \bar{U}}{\partial y} = -\frac{\partial(\overline{u'v'})}{\partial y} - \frac{\partial(\overline{u'^2} - \overline{v'^2})}{\partial x}. \tag{1}$$

Each of the terms in Eq. (1) can be measured and Fig. 8 presents cross-stream profiles as obtained in the ZPG asymmetric wake at the sample location $x/\theta_0 = 38$. For reference, this figure also shows the local wake mean velocity profile. Both the lateral advection and the normal stress terms are small in comparison with the corresponding streamwise term. Hence, to good approximation,

$$\bar{U}\frac{\partial \bar{U}}{\partial x} \approx -\frac{\partial(\overline{u'v'})}{\partial y}. \tag{2}$$

Figure 8 shows that as a consequence of the cross-stream asymmetry of the Reynolds stress distribution, the peak streamwise mean velocity gradient does not occur at the lateral location associated with $U_d(x)$ (as is the case for the *symmetric* wake). Rather, the peak value of $\partial U/\partial x$ may be observed to occur at a lateral location just inside the thinner wake shear layer. Near the lateral location of maximum velocity defect, the mean velocity U will exhibit a larger increment at downstream locations within the thinner shear layer. In the thicker shear layer, U will have a smaller increment. As a consequence, this will give rise to the observed lateral migration of the location of maximum velocity defect toward the thicker shear layer as the wake evolves in x. In this manner, the observed streamwise variation of $y_d(x)$ is directly related to the asymmetry of the Reynolds stress in the wake.

The streamwise variation of the local maximum velocity defect for the symmetric and asymmetric ZPG wakes is compared in Fig. 9 (along with nonzero pressure gradient cases which will be discussed in the next section). In each case the maximum local defect U_d is normalized by the initial maximum defect value $(U_d)_{x_0}$ in order to account for the initial difference in defect magnitude for the two cases. For the ZPG case, Fig. 9 shows that there is essentially no difference in the velocity defect decay rate between the symmetric and asymmetric cases with both tending to an $x^{-1/2}$ variation.

2. Effect of pressure gradient on wake mean flow development

Figure 9 compares the streamwise variation of the normalized maximum velocity defect $U_d/(U_d)_{x_0}$ for the ZPG, APG, and FPG cases. It is apparent from this figure that wake asymmetry has virtually no effect on the defect decay rate. The streamwise variation of the velocity defect exhibits a virtually identical dependence on imposed pressure gradient for corresponding symmetric and asymmetric cases. It is also clear from Fig. 9 that the imposed pressure gradient has a pronounced effect on the wake defect decay. As noted earlier, the maximum defect for the zero pressure gradient case exhibits the expected $x^{-1/2}$ variation. The velocity defect decay is significantly reduced by imposition of the adverse pressure gradient. In fact, it may be noted that for the APG case the velocity defect actually grows slightly at the largest x locations measured. In contrast, for the FPG case the velocity defect decays much more rapidly than for the ZPG wake.

Figure 10 summarizes the effect of applied constant pressure gradient on wake spreading for both the symmetric and asymmetric wakes. In particular, this figure presents the streamwise variation of the normalized wake width, $\delta(x)/\theta_0$, for zero, favorable, and adverse pressure gradient conditions. The streamwise location at which the pressure

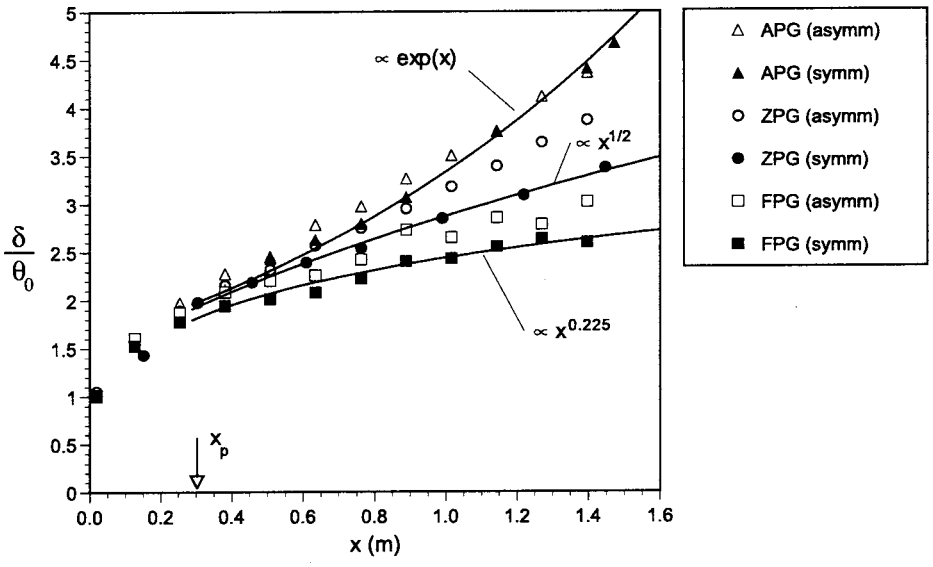

FIG. 10. Streamwise variation in wake spreading for the symmetric and asymmetric wakes.

gradient is first applied is indicated on the abscissa as x_p. The profound effect of the pressure gradient on wake spreading is readily apparent from this figure. Figure 10 shows that for both the symmetric and asymmetric wakes in FPG, the wake widening is reduced below that for the ZPG. As was the case for ZPG, however, the asymmetric wake in FPG widens at a greater rate than the corresponding symmetric case. For both symmetric and asymmetric FPG cases, the wake width appears to follow a power law variation with x but with reduced exponent from the asymptotic value of 1/2 that characterizes the zero pressure gradient case. The symmetric wake adverse pressure gradient case is observed to widen approximately exponentially with x as evidenced by the indicated least-squares fit. Initially the asymmetric, APG wake widens at a slightly greater rate than that exhibited by the symmetric case. However, by $x \approx 1.25$ m the two cases are virtually indistinguishable. Hence, unlike the ZPG case discussed earlier, the symmetric and asymmetric APG wakes exhibit virtually identical streamwise growth except immediately downstream of x_p.

Note that in both Figs. 9 and 10 the response of the mean flow to the imposed pressure gradient is very rapid with both δ and U_d showing deviations from the ZPG case immediately downstream of imposition of the pressure gradient at x_p.

Figure 11 compares measured symmetric wake mean velocity defect profiles in zero, favorable, and adverse pressure gradients at representative streamwise locations. The local velocity defect $U_e - \overline{U}$ is scaled by U_d while the lateral spatial coordinate is scaled with $\delta(x)$. Using this scaling, it is apparent that the symmetric wake mean velocity profiles exhibit similarity and are nearly universal in shape despite the different imposed pressure gradients. In each case the measurements in Fig. 11 conform quite well to the profile of form

$$\frac{U_e - \overline{U}}{U_d} = \exp[-0.637(y/\delta)^2 - 0.056(y/\delta)^4] \qquad (3)$$

which is identical to that used by Wynganski *et al.*[21] to collapse wake profiles generated by screens, cylinders, and airfoils under zero pressure gradient conditions. Rogers[13] also reports a nearly universal mean velocity profile shape for DNS simulations of planar turbulent wakes involving constant positive and negative imposed streamwise strain rates. In an actual high-lift flow field, the outermost wake-like portion of the main element confluent boundary layer exhibited self-similarity despite the strong adverse pressure gradient environment as reported by Thomas *et al.*[16]

In order to assess the degree of similarity exhibited by the asymmetric wake mean velocity, a similar but modified scaling was employed. This involved examining the scaled velocity defect $f \equiv (U_e - \overline{U})/U_d$ as a function of $\eta \equiv (y - y_d)/\delta_i$, $i = 1, 2$. Here $y_d(x)$ denotes the lateral location of maximum velocity defect, and $\delta_1(x)$ and $\delta_2(x)$ denote the half-widths of the thick and thin wake shear layers, respectively. In effect, for the asymmetric wake, we examine the

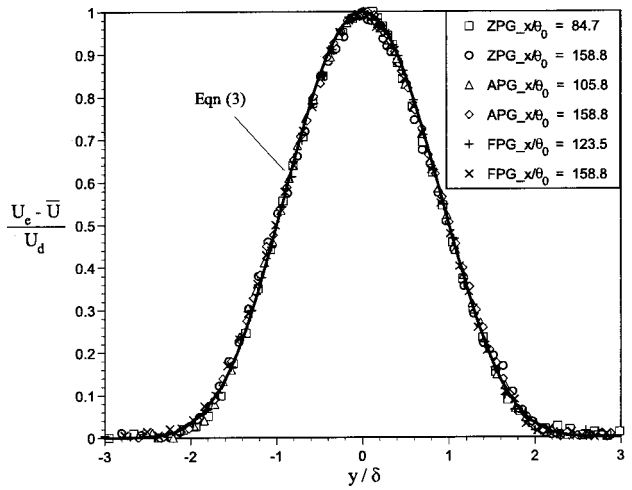

FIG. 11. Scaled symmetric wake velocity defect profiles for APG, ZPG, and FPG cases.

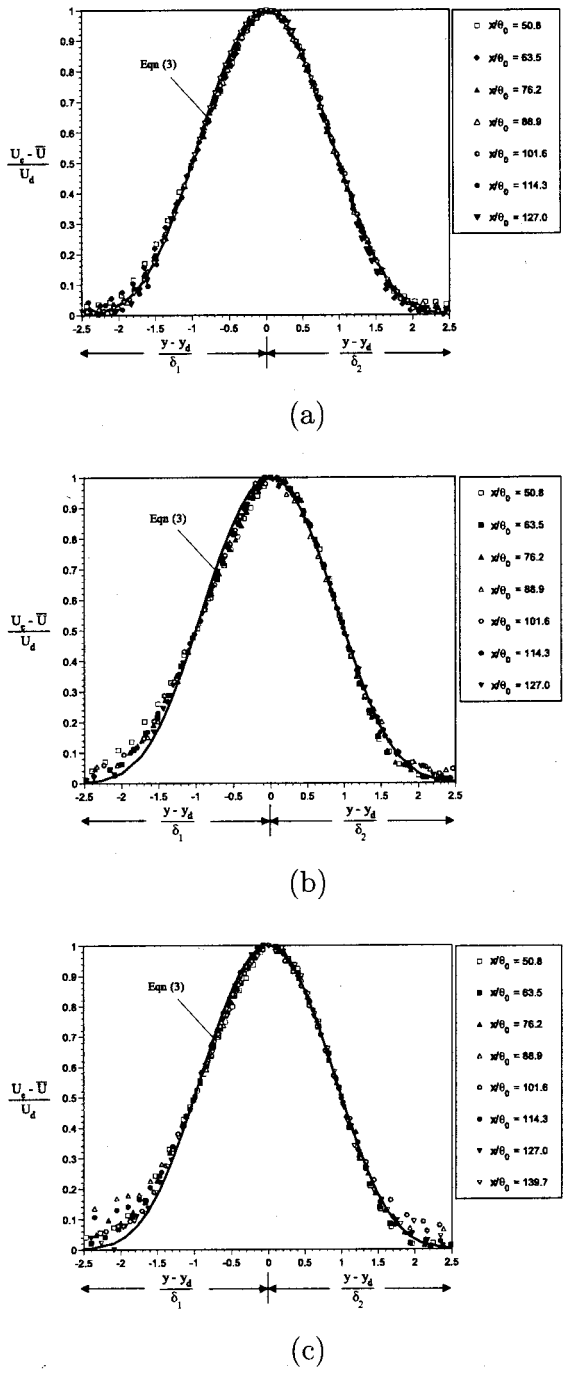

FIG. 12. Scaled asymmetric wake velocity defect profiles. (a) APG case; (b) ZPG case; and (c) FPG case.

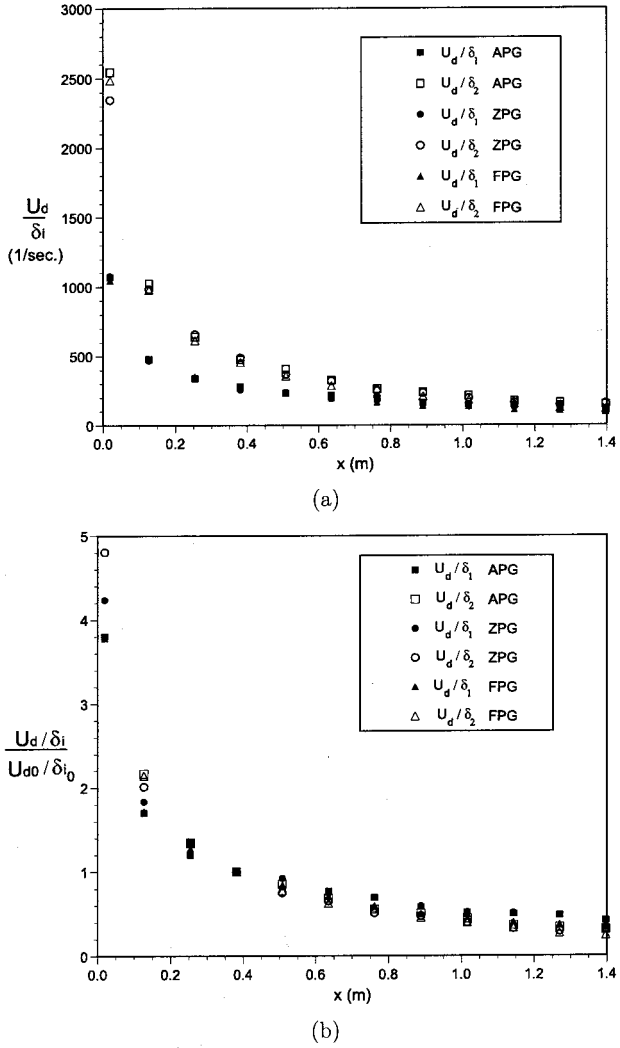

FIG. 13. Streamwise variation of U_d/δ_i for asymmetric wake in different pressure gradient cases.

similarity of the two wake shear layers individually. Figure 12 presents scaled asymmetric wake velocity defect profiles corresponding to the APG, ZPG, and FPG cases as obtained at selected streamwise locations throughout the diffuser. It is apparent that this scaling provides a reasonably good collapse of the profiles at each streamwise location. Figure 12 implies that the asymmetric wake shear layers exhibit similarity provided that their disparate streamwise growth rates $(d\delta_2/dx > d\delta_1/dx)$ are accounted for in the scaling. Also shown in Fig. 12 is the profile shape given by (3) which was found to accurately represent the scaled symmetric wake defect profiles. For each pressure gradient condition shown in Fig. 12 the thin wake shear layer $(y-y_d>0)$ conforms very well to (3) while some deviation may be noted for the thicker wake shear layer $(y-y_d<0)$. In fact, it turns out that the thick shear layer is better fit to a simpler profile shape given by $(U_e-\overline{U})/U_d=\exp[-0.637(y/\delta_i)^2]$. Comparison with (3) indicates that in each case the scaled asymmetric wake defect profiles are not completely symmetric. The deviation from symmetry is smallest for the APG case but the overall effect of pressure gradient on profile shape appears to be small. Rather, the slight asymmetry in the scaled profiles appears to originate from the disparate initial conditions in the upper and lower wake shear layers. Despite this, the wake profiles have been rendered nearly symmetric with the applied scaling and this is reminiscent of the results of Wynganski *et al.*[21] where different widening rates were measured for different wake-generating bodies (initial conditions) although the scaled wake mean velocity defect profiles appeared to exhibit a common self-preserving shape.

Figure 13 presents the streamwise evolution of the ratio U_d/δ_i for the thin and thick asymmetric wake shear layers as

measured for each of the pressure gradient cases. This quantity is directly proportional to the absolute value of the maximum local mean strain rate $|\partial U/\partial y|_{\max}$. In particular, for the scaled defect profile $f(\eta)$ shown in Fig. 12, the local maximum strain rate $|\partial U/\partial y|_{i,\max}=(U_d/\delta_i)|f'|_{\max}$. The streamwise evolution of U_d/δ_i shown in Fig. 13(a) tends to group into two curves; one for each of the wake shear layers. Furthermore, the two groups of curves tend to merge as the asymmetric wake develops downstream. Of particular importance is the observation that the streamwise variation of U_d/δ_i is virtually identical (within measurement uncertainty) for each pressure gradient case. This may seem surprising given the very significant differences in the streamwise evolution of $\delta_i(x)$ and $U_d(x)$ shown previously. In order to understand this note that, to good approximation, the mean spanwise vorticity $\Omega_z \approx -1/2\partial U/\partial y$. Upstream of imposition of the pressure gradient the mean spanwise vorticity is identical in each case, consistent with maintenance of the same initial conditions. The Reynolds-averaged vorticity transport equation shows that the redistribution of spanwise vorticity will be independent of the direct effects of the imposed pressure gradient ($\nabla\times\nabla P=0$). Physically, this is a consequence of the fact that pressure forces act through the centroid of fluid elements. As expected, Fig. 13(a) also shows initially higher strain rates in the thinner wake shear layer. For both wake shear layers the strain rate diminishes with streamwise distance and values in the thin and thick shear layer are observed to approach each other as the mean flow becomes more symmetric with streamwise distance. In fact, if U_d/δ_i is normalized by the initial strain rate to account for the initial difference, the two groups of curves in Fig. 13(a) collapse to one, as shown in Fig. 13(b). The imposed pressure field clearly has no direct effect on the mean strain rate. Similar results are shown in Fig. 10 of Liu *et al.*[15] for the symmetric turbulent wake in pressure gradient.

B. Wake turbulent flow development

One of the most physically descriptive measures by which the effect of pressure gradient on the turbulent flow may be assessed is the streamwise evolution of the turbulent kinetic energy per unit mass, $k\equiv 1/2(\overline{u'^2}+\overline{v'^2}+\overline{w'^2})$. Using x-wire measurements, profiles of the required normal stresses were measured over a range of streamwise locations and the local turbulent kinetic energy computed. Figure 14 compares cross-stream profiles of k for the APG and FPG cases as obtained at representative streamwise locations in the asymmetric wake. For reference, corresponding k profiles for the ZPG case are also shown at the same locations. The lateral coordinate y has been left unscaled in order that the associated effect of pressure gradient on wake widening may also be observed. Figure 14(a) shows that upstream of x_p the turbulent kinetic energy profiles are virtually identical due to matching initial conditions. The turbulent kinetic energy is initially higher in the thick wake shear layer due to the disparate boundary layer development that occurs over the top and bottom surfaces of the wake-generating plate (this is associated with the flow control used to generate the initial wake asymmetry). Figure 14 shows that, along with the enhanced lateral wake growth, the APG condition sustains higher levels of turbulent kinetic energy over larger streamwise distances than does the FPG wake. In contrast, the FPG case exhibits a more rapid streamwise decay of turbulence kinetic energy than the ZPG case. A similar effect of pressure gradient on turbulence kinetic energy levels was reported for the symmetric wake as described in Liu *et al.*[15] Figure 14 also shows that as the asymmetric wake evolves in x, the local turbulence kinetic energy profiles gradually become more symmetric in y. The rate at which cross-stream symmetry is approached clearly depends on the applied pressure gradient. In particular, the APG case approaches a symmetric cross-stream distribution of k much more rapidly than does the FPG case which still exhibits a degree of asymmetry at the last measurement station shown in Fig. 14(f). These data suggest an accelerated development of the turbulence for the APG case.

For the wake in pressure gradient, turbulence kinetic energy production involves not only the local shear production terms, $-\overline{u'v'}\partial U/\partial y$ and $-\overline{u'v'}\partial V/\partial x$, but also the dilatational production term, $-(\overline{u'^2}-\overline{v'^2})\partial U/\partial x$. Measurements show that $\overline{u'^2}>\overline{v'^2}$, so the dilatational term is positive for the APG case and represents an additional source for turbulence. For the FPG case, the term is negative and represents the transfer of turbulent kinetic energy back to the mean flow. The shear production term, $-\overline{u'v'}\partial V/\partial x$, was measured and, as expected, was found to be entirely negligible in each case since $\partial U/\partial y \gg \partial V/\partial x$. Comparisons between measured cross-stream profiles of the local dilatational and shear turbulence production terms show that, for both APG and FPG cases, the wake flow is shear dominated despite the imposed streamwise pressure gradients. An example is shown in Fig. 15 which compares measured profiles of local shear production, $-\overline{u'v'}\partial U/\partial y$, and dilatational production, $-(\overline{u'^2}-\overline{v'^2})\partial U/\partial x$, as obtained at $x/\theta_0=101.5$ for the asymmetric wake FPG case. The dominance of the local shear production term is apparent. This was also the case in the symmetric wake as well, since the imposed pressure gradients were the same. Note, however, that the dominance of the shear production does not preclude the dilatational production mechanism from playing an important role in the turbulent wake development. As described in Liu *et al.*[15] the dilatational production can serve as a trigger to initiate pressure gradient-dependent differences in the turbulent kinetic energy and consequently, an associated disparity in the Reynolds shear stress between different pressure gradient cases. More will be said about this later in this section of the paper.

Figure 16 presents the streamwise evolution of the total turbulence production (dilatational plus shear) as measured at the (arbitrary) lateral locations $y/\delta_i=\pm 0.9$ in the thick and thin asymmetric wake shear layers for the FPG and APG cases. In each case the turbulence production decreases with streamwise distance. This reduction is consistent with the streamwise variation in U_d/δ_i (a quantity intimately related to the maximum mean strain rate, $\partial U/\partial y$) shown in Fig. 13. For both pressure gradients the magnitude of the turbulence production in the thin shear layer is always higher. However, this disparity is reduced as the asymmetric wake develops

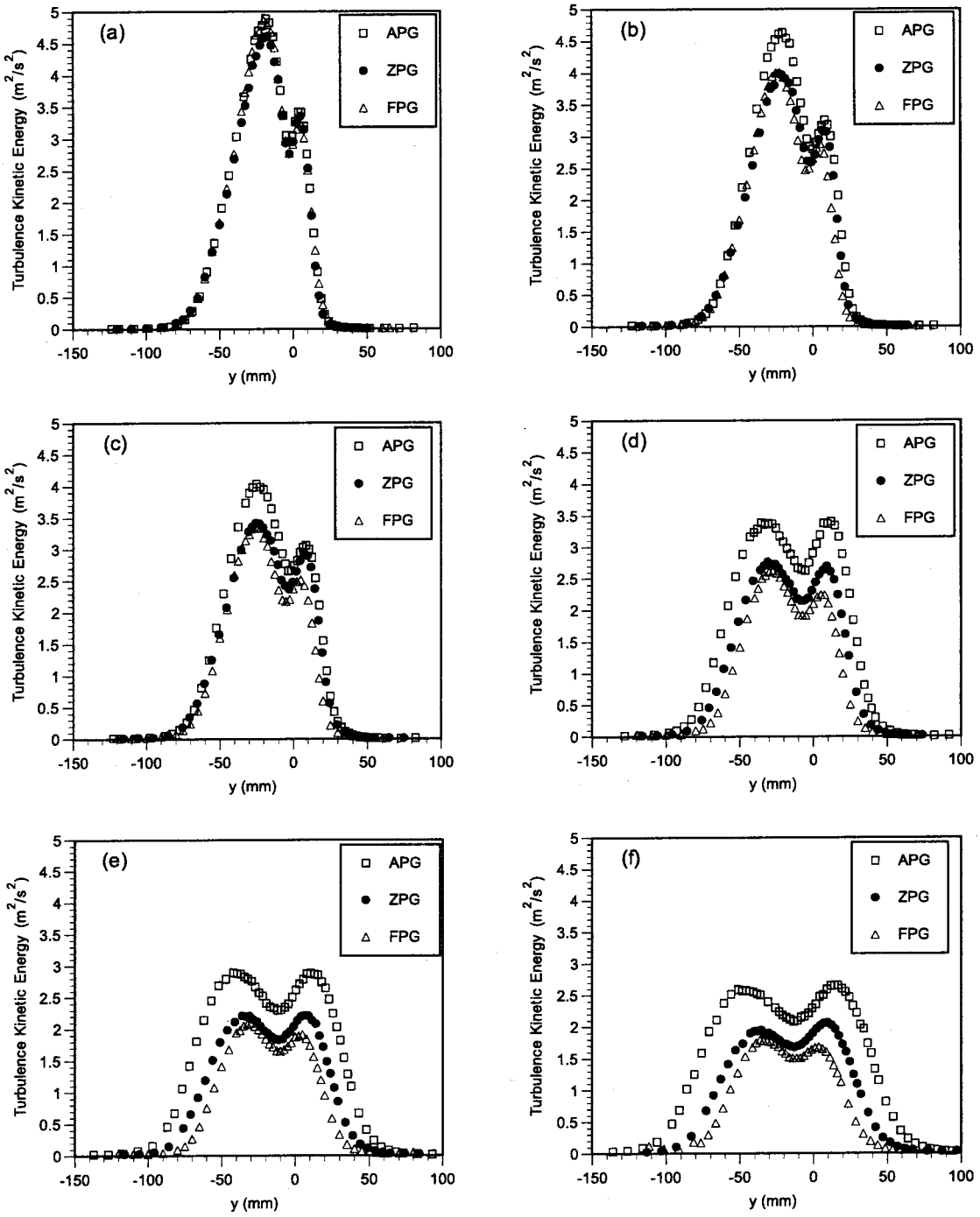

FIG. 14. Streamwise evolution of turbulent kinetic energy for the asymmetric wake: (a) $x/\theta_0 = 25.4$; (b) 38.1; (c) 50.8; (d) 76.2; (e) 101.6, and (f) 127.

downstream. This is associated with local mean velocity profiles becoming more symmetric with streamwise distance. Note also that at any streamwise location, the turbulence production associated with the APG case exceeds that for the FPG case. In addition, Fig. 16 shows that the effect of applied pressure gradient on turbulence production is greatest in the thin wake shear layer. That is, the difference in local turbulence production between the APG and FPG cases is most significant in the thinner wake shear layer.

As demonstrated previously in Fig. 13, the mean strain rate $\partial U/\partial y$ is not directly affected by the applied streamwise pressure gradient. It has also been shown that the wake is shear dominated and greater local turbulence production rates in the thin shear layer (associated with higher $\partial \overline{U}/\partial y$) will give rise to the gradual return to cross-stream symmetry in the turbulence kinetic energy profiles shown in Fig. 14. However, it remains to account for the pressure gradient-dependent differences shown in both Fig. 14 and in the streamwise evolution of turbulence production shown in Fig. 16. In order to account for these results we must have pressure gradient-dependent differences in the Reynolds stresses and we next describe how these can occur.

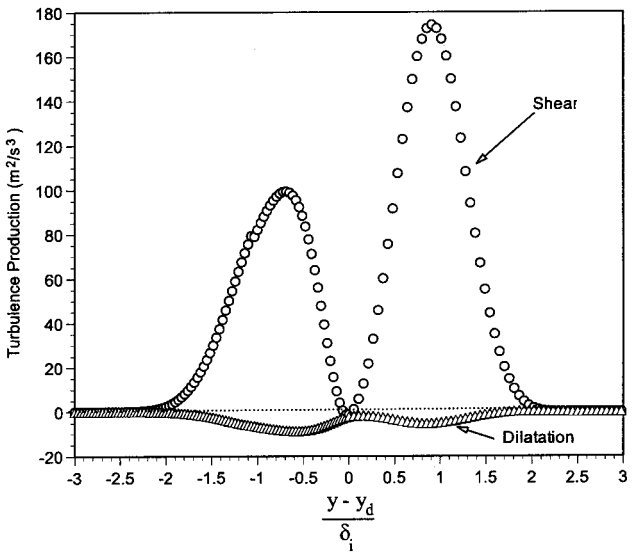

FIG. 15. Comparison of shear and dilatational turbulence production at $x/\theta_0 = 101.5$ for the asymmetric wake FPG case.

Due to the maintenance of the same initial conditions, both the wake mean flow and turbulence statistics are initially identical (within experimental uncertainty) upstream of the location x_p where the constant pressure gradient is initially imposed. Although we have shown that the wake turbulence development is shear dominated, the dilatational terms play an essential role in initiating pressure gradient-dependent differences in the Reynolds stresses. For example, the production terms in the Reynolds stress transport equation $D(\overline{u'v'})/Dt$ are

$$-\left[\overline{u'^2}\frac{\partial \overline{V}}{\partial x}+\overline{v'^2}\frac{\partial \overline{U}}{\partial y}+\overline{u'v'}\left(\frac{\partial \overline{U}}{\partial x}+\frac{\partial \overline{V}}{\partial y}\right)\right] = -\overline{u'^2}\frac{\partial \overline{V}}{\partial x}-\overline{v'^2}\frac{\partial \overline{U}}{\partial y}.$$

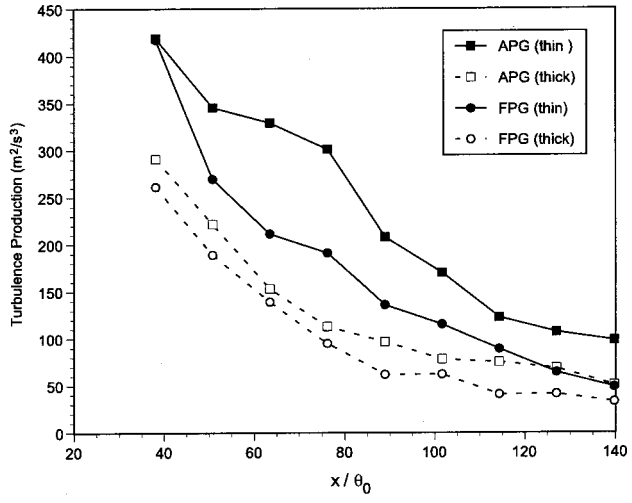

FIG. 16. Streamwise evolution of turbulence production for the asymmetric wake APG and FPG cases at $y/\delta_i = \pm 0.9$.

Here $-\overline{v'^2}\partial \overline{U}/\partial y$ is obviously the dominant production term since $\partial U/\partial y \gg \partial V/\partial x$ and $\overline{u'^2} \sim O(\overline{v'^2})$. Since the strain rate $\partial U/\partial y$ is not dependent on pressure gradient we must consider how the normal stress, $\overline{v'^2}$, can take on pressure gradient-dependent differences that could ultimately influence the Reynolds stress production. Examining the source terms in the $D(\overline{v'^2})/Dt$ transport equation we have

$$-2\left(\overline{u'v'}\frac{\partial \overline{V}}{\partial x}+\overline{v'^2}\frac{\partial \overline{V}}{\partial y}\right)$$

and the dominant term is $-\overline{v'^2}\partial \overline{V}/\partial y$ which is directly related to the applied pressure gradient through conservation of mass ($\partial V/\partial y = -\partial U/\partial x$). It is apparent therefore, that $\overline{v'^2}$ will be augmented for the FPG case (a consequence of the "spin-up" associated with the stretching of streamwise vorticity) and for the APG case it will be reduced. This would suggest that the dominant source term in the Reynolds stress transport equation, $-\overline{v'^2}\partial \overline{U}/\partial y$, should enhance the production of $-\overline{u'v'}$ for the FPG case relative to the APG case. The effect of this would, in fact, be counter to the results shown in Figs. 14 and 16. The resolution of this apparent conflict comes from considering the source terms in the $D(\overline{u'^2})/Dt$ transport equation where we have

$$-\left(\overline{u'^2}\frac{\partial \overline{U}}{\partial x}+\overline{u'v'}\frac{\partial \overline{U}}{\partial y}\right).$$

Hence, in contrast to the previous results for the lateral fluctuating component, $\overline{u'^2}$ will be augmented for the APG case and reduced for FPG. While $\overline{u'^2}$ does not explicitly appear as a source term for the production of $-\overline{u'v'}$, it is important to realize that a portion of the kinetic energy initially appearing in the streamwise fluctuation will be redistributed to the $\overline{v'^2}$ and $\overline{w'^2}$ components due to the role of fluctuating pressure in the velocity-pressure-gradient tensor, more specifically, the pressure-rate-of-strain tensor. As a consequence, the gain in $\overline{v'^2}$ due to the redistribution of augmented $\overline{u'^2}$ under the APG condition can actually exceed the direct production of $\overline{v'^2}$ under the FPG condition. This would, in turn, lead to enhanced growth of the Reynolds stress for the APG case. The enhanced Reynolds stress $-\overline{u'v'}$ would again strengthen the production of the normal stress $\overline{u'^2}$ as revealed by the production term $-\overline{u'v'}\partial \overline{U}/\partial y$ in the $D(\overline{u'^2})/Dt$ transport equation. This appears to be the case as shown in Fig. 17 which compares profiles of $-\overline{u'v'}$ at three selected streamwise locations for the FPG and APG asymmetric wake. Near x_p the profiles are nearly identical. Farther downstream, $-\overline{u'v'}$ decays at a slower rate for the APG case than for FPG. In fact, at certain x locations $-\overline{u'v'}$ even shows streamwise growth for the APG case. In each case the effect is greater in the thin shear layer and this is a manifestation of the importance of strain rate in the dominant source term in the Reynolds stress transport equation, $-\overline{v'^2}\partial \overline{U}/\partial y$.

Hence, even though the wake is shear dominated, pressure gradient-dependent differences in the local Reynolds stress have their origin in dilatational terms. Once created, these disparities in Reynolds stress give rise to significant

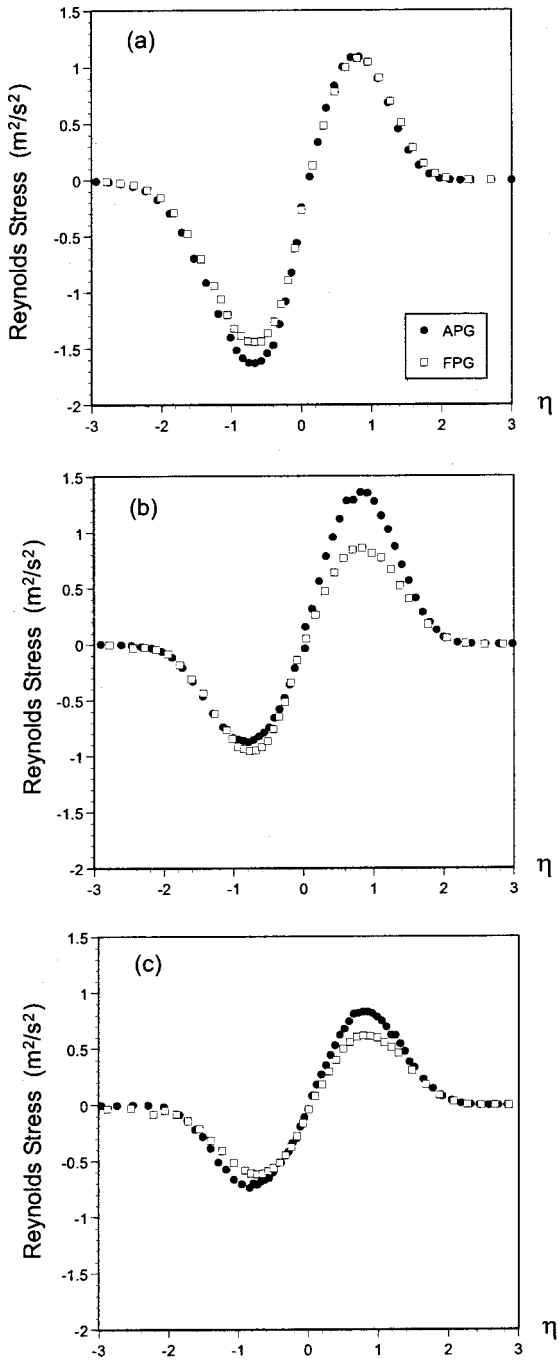

FIG. 17. $-\overline{u'v'}$ at representative streamwise locations for the asymmetric wake under APG and FPG conditions: (a) $x/\theta_0 = 38.1$; (b) 76.2; and (c) 127.

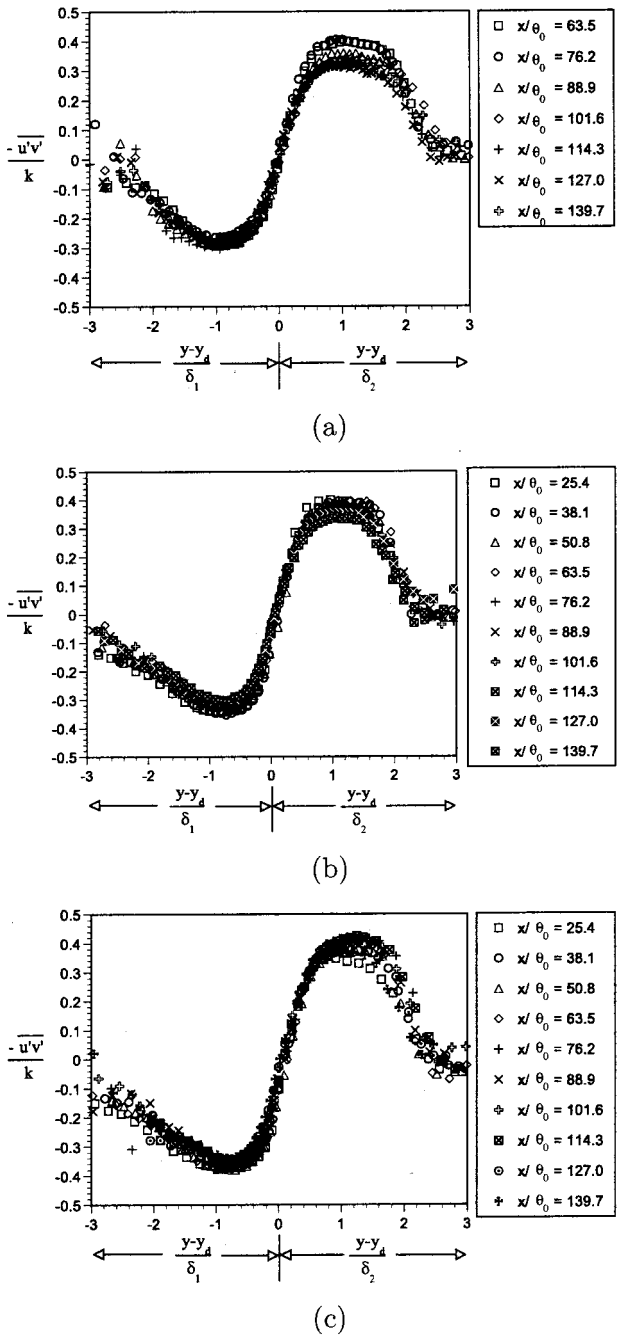

FIG. 18. Cross-stream profiles of $-\overline{u'v'}/k$ for the APG, ZPG, and FPG asymmetric wake cases: (a) APG case; (b) ZPG case; and (c) FPG case.

differences in shear turbulence production that are largely responsible for the observed effect of pressure gradient on the turbulent kinetic energy. Additional evidence of this comes from examination of the streamwise variation in the difference between local turbulence production rates for the APG and FPG cases, $\Delta_e(x)$. This will be composed of differences due to dilatational production, $\Delta_d(x)$, as well as those due to shear production, $\Delta_s(x)$. It is found that immediately downstream of x_p, $\Delta_d/\Delta_e \gg \Delta_s/\Delta_e$ while farther downstream, Δ_s/Δ_e dominates. This is consistent with the argument that the pressure gradient-dependent effects on the turbulent field are initiated by dilatational terms that give rise to subsequent modification in the turbulent shear production via changes in the Reynolds stress.

For the symmetric wake in pressure gradient, Liu *et al.*[15] demonstrated that cross-stream Reynolds stress profiles exhibit a reasonable collapse when scaled by k. This property of the Reynolds stress is also observed for the asymmetric wake in each of the different pressure gradient cases. Figure 18 presents asymmetric wake $-\overline{u'v'}/k$ profiles for APG, ZPG, and FPG conditions. In each case it is clear that scaling the Reynolds stress by k provides a reasonable collapse. The peak magnitude of the Reynolds stress varies between approximately $0.3k$ and $0.4k$. That $-\overline{u'v'}$ scales with k is

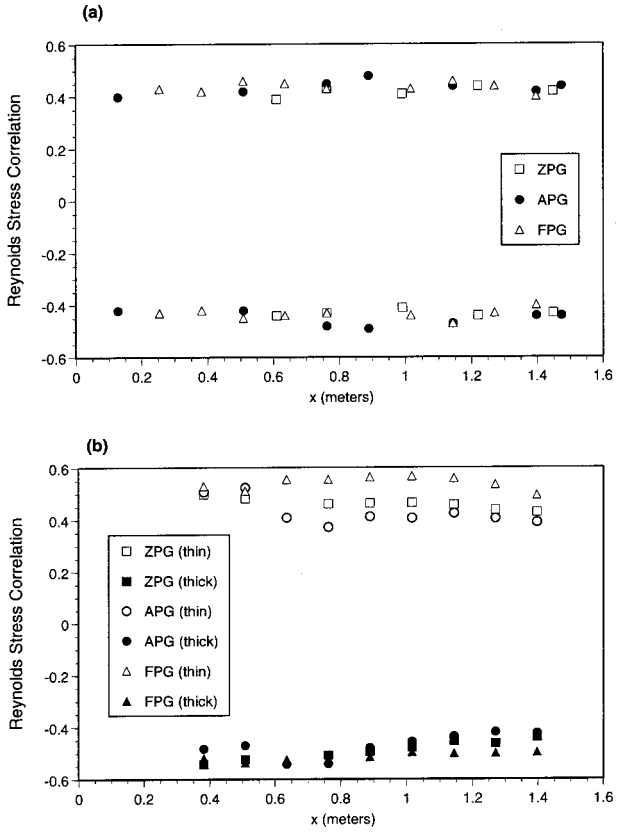

FIG. 19. Streamwise evolution of the Reynolds stress correlation: (a) symmetric wake and (b) asymmetric wake.

equivalent to stating that the b_{uv} component of the anisotropy tensor is nearly invariant with respect to the streamwise coordinate. This indicates that the neglect of variations in $-\overline{u'v'}$ that are due to the anisotropy tensor while retaining those due to k is a very reasonable approximation for the strained turbulent wake flow. This has important implications regarding the applicability of algebraic Reynolds stress closure models to this class of strained flows. Inherent to the algebraic stress model originally proposed by Rodi is the so-called "weak-equilibrium assumption,"[22]

$$\frac{\overline{D}}{Dt}(\overline{u_i'u_j'}) \approx \frac{\overline{u_i'u_j'}}{k}\frac{\overline{Dk}}{Dt}, \tag{4}$$

which is equivalent to assuming that $\overline{D}/\overline{Dt}(\overline{u_i'u_j'}/k)=0$. For the wake flow under investigation here, it is clear from Fig. 18 that if the lateral coordinate is scaled by δ_i then $\partial(\overline{u_i'u_j'}/k)/\partial x \approx 0$ for both favorable and adverse gradients. Measurements confirm that $\overline{V}\partial(\overline{u_i'u_j'}/k)/\partial y$ is generally quite small across the wake as well.

Figure 19 presents the streamwise evolution of the Reynolds stress correlation, $\rho_{uv}=-\overline{u'v'}/\sqrt{\overline{u'^2}}\sqrt{\overline{v'^2}}$, as measured at $y/\delta_i=\pm 0.95$ (i.e., near the location of maximum mean strain rate) for both the symmetric and asymmetric wakes in pressure gradient. For the symmetric wake, Fig. 19(a) shows that ρ_{uv} is essentially independent of pressure gradient and there is very little streamwise variation with $|\rho_{uv}| \approx 0.44$ in each case. Corresponding measurements for the asymmetric wake in pressure gradient are shown in Fig. 19(b). For the asymmetric wake there is little effect of pressure gradient on ρ_{uv} for the thick shear layer. Initially, $\rho_{uv} \approx -0.5$ but appears to gradually approach values comparable to those in the symmetric wake near the end of the test section. In contrast, the evolution of ρ_{uv} in the thin wake shear layer exhibits a significant effect of applied pressure gradient. Upstream of x_p we see that $\rho_{uv} \approx 0.5$ for each case. However, downstream of x_p the evolution of ρ_{uv} is distinctly different depending on the applied pressure gradient. In particular, the APG case appears to exhibit the most rapid development with ρ_{uv} becoming nearly constant by $x \approx 0.9$ m. In contrast, the value for the FPG case is clearly still evolving at the last measurement station.

Figure 20 presents the evolution of cross-stream profiles of the rms stream-wise velocity fluctuation for both the symmetric [(a)–(c)] and asymmetric [(d)–(f)] wakes under APG, ZPG, and FPG conditions. The rms fluctuations have been scaled in the traditional manner by the local maximum velocity defect, $U_d(x)$, and the lateral coordinate (relative to y_d) by the wake shear layer thickness δ_i. Figure 20 shows that for both the symmetric and asymmetric wakes, this traditional scaling fails to collapse the wake $\sqrt{\overline{u'^2}}/U_d$ profiles, indicating that the evolution of the turbulent field does not keep pace with the changes in the mean flow. Hence the similarity exhibited in Figs. 11 and 12 is incomplete. The lack of collapse of the $\sqrt{\overline{u'^2}}$ profiles is not surprising since the experiment is focused on the near wake and it is typical for mean flow similarity to occur before similarity of second-order turbulence statistics is reached. For example, even in the absence of applied pressure gradient, the $\sqrt{\overline{u'^2}}/U_d$ profiles for the symmetric wake [Fig. 20(b)] are just beginning to show collapse near the end of the test section. However, Fig. 20 shows that the degree of collapse exhibited by the $\sqrt{\overline{u'^2}}$ profiles depends strongly on the imposed pressure gradient. The overall impression one is left with is that the APG case provides an accelerated approach to an eventual self-similar state. The collapse exhibited by the APG symmetric case is especially notable. In contrast, the FPG case shows no evidence of collapse as the mean velocity defect U_d apparently decreases at a greater rate than does $\sqrt{\overline{u'^2}}$. In comparing the symmetric and asymmetric cases for a given pressure gradient condition, care must be used since the range of x/θ_0 covered by the flow apparatus is not the same. Recall that this is due to the disparate initial conditions in the two cases. However, even after taking this into account it does appear that wake asymmetry delays the approach to self-similarity over that observed in the symmetric wake. This is most obvious by comparing the symmetric and asymmetric APG case over a comparable range of x/θ_0.

Wake similarity scaling issues

The similarity exhibited at the level of the mean flow as shown in Figs. 11 and 12, respectively, suggests that it may be possible to collapse the corresponding Reynolds stress

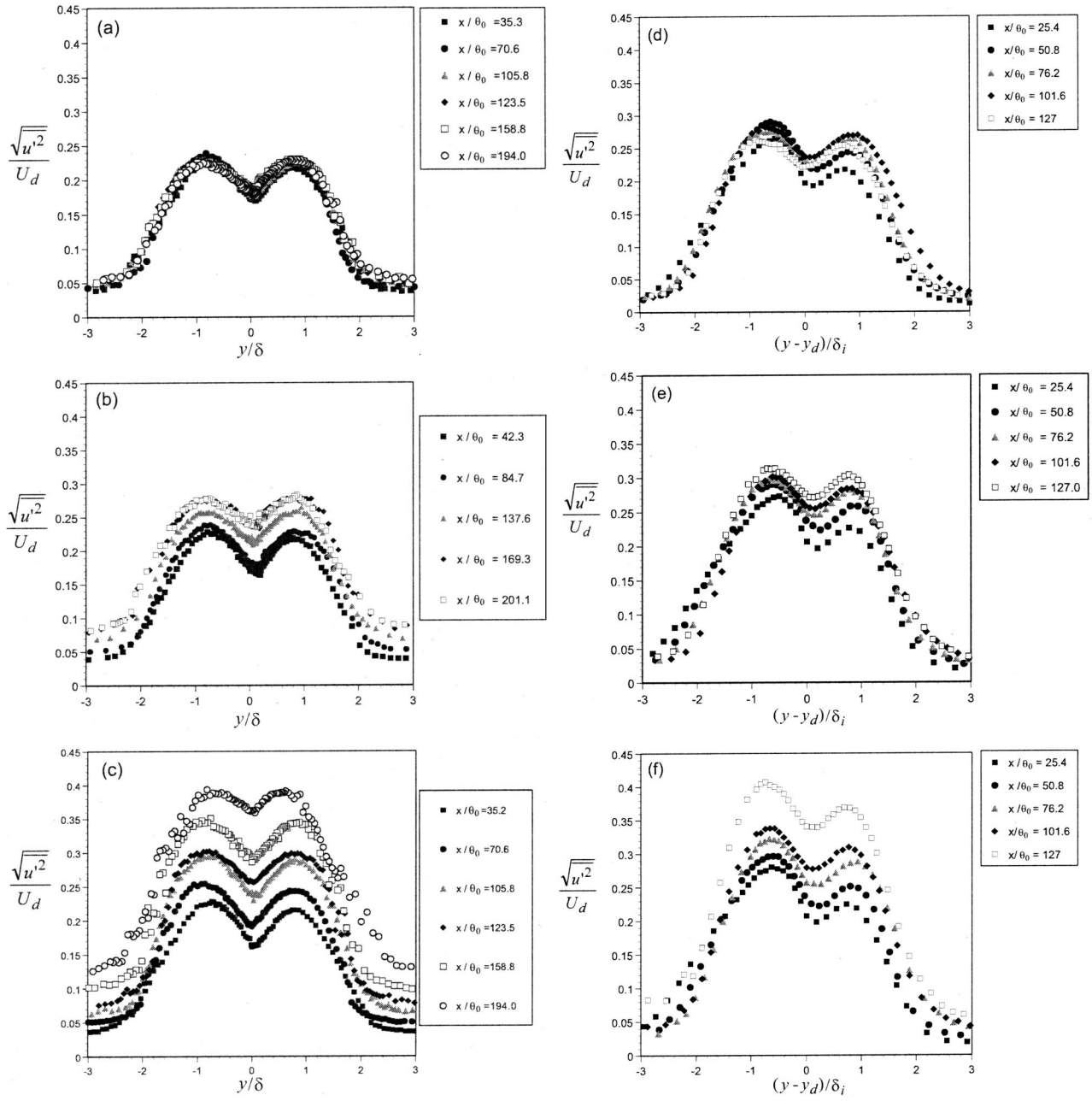

FIG. 20. Cross-stream profiles of $\sqrt{\overline{u'^2}}/U_d$ at several representative streamwise locations. (a) Symmetric wake APG case; (b) symmetric wake ZPG case; (c) symmetric wake FPG case; (d) asymmetric wake APG case; (e) asymmetric wake ZPG case; and (f) asymmetric wake FPG case.

$-\overline{u'v'}$ profiles by suitable scaling. It has already been demonstrated that the similarity exhibited by the wake is incomplete. In addition, although not presented here, classical scaling of the Reynolds stress by $U_d^2(x)$ failed to produce a suitable collapse. In this section, we examine the conditions required for similarity at the level of the momentum equation.

The governing equation for the flow is the thin shear layer form of the momentum equation,

$$\overline{U}\frac{\partial \overline{U}}{\partial x}+\overline{V}\frac{\partial \overline{U}}{\partial y}=U_e\frac{dU_e}{dx}-\frac{\partial(\overline{u'v'})}{\partial y}, \tag{5}$$

and mass conservation,

$$\frac{\partial \overline{U}}{\partial x}+\frac{\partial \overline{V}}{\partial y}=0. \tag{6}$$

By substituting $f(\eta)\equiv(U_e-\overline{U})/U_d$ and $g(\eta)\equiv-\overline{u'v'}/R(x)$ [where $\eta\equiv(y-y_d)/\delta_i$ and $R(x)$ is an unspecified, x-dependent Reynolds stress scaling] into the x-momentum equation, it is straightforward to show that the governing equation becomes

$$Af+Bf^2+C\eta f'+Df'\int_0^\eta f\ d\eta+Ef'=R(x)g', \tag{7}$$

where

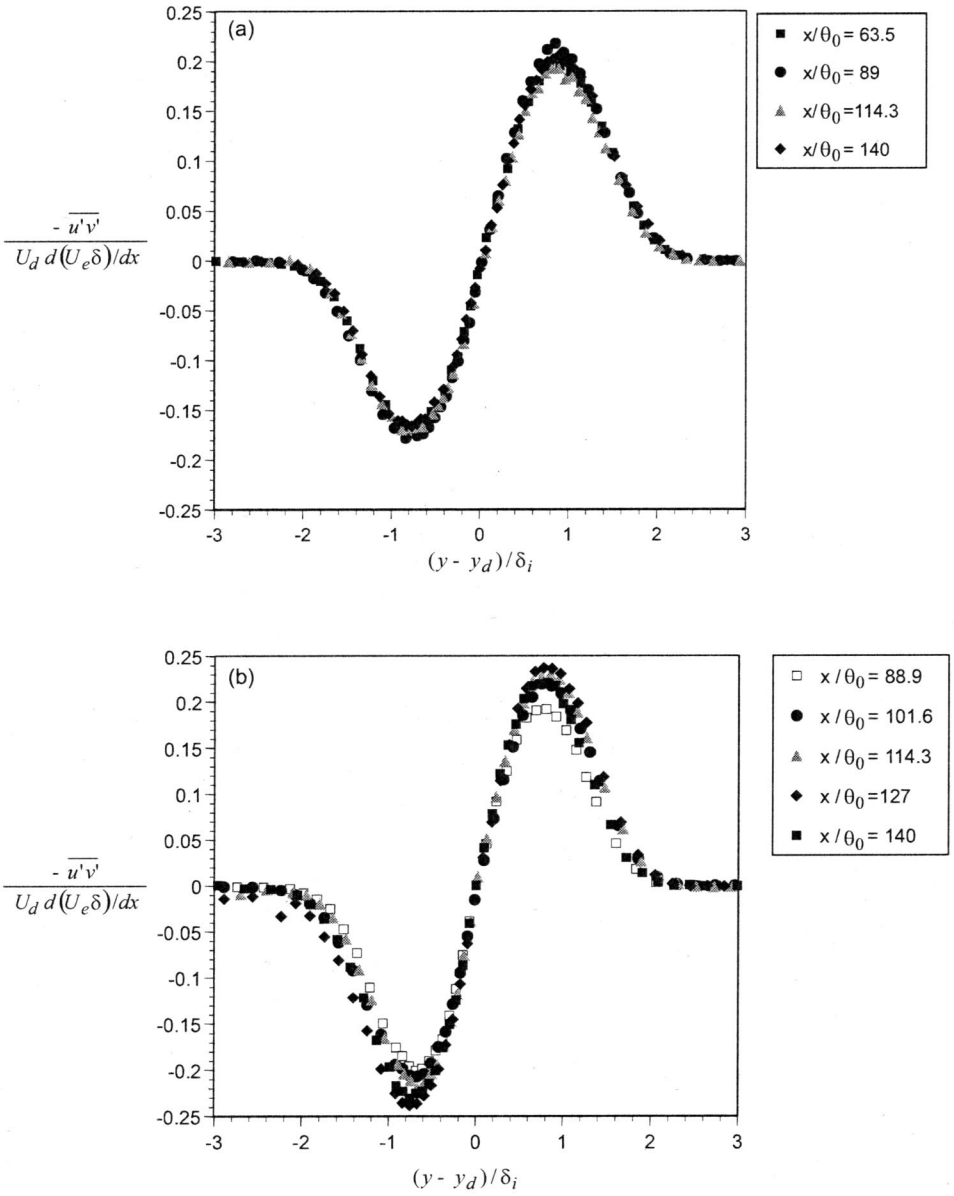

FIG. 21. Scaled asymmetric wake Reynolds stress profiles: (a) APG case and (b) FPG cases.

$$A=-\left[\delta_i\frac{d(U_eU_d)}{dx}\right],\quad B=\left[\delta_iU_d\frac{dU_d}{dx}\right],$$

$$C=\left[U_d\frac{d(U_e\delta_i)}{dx}\right],\quad D=-\left[U_d\frac{d(U_d\delta_i)}{dx}\right],$$

$$E=\left[U_eU_d\frac{dy_d}{dx}\right].$$

For the symmetric wake $E=0$ (since $y_d=0$) and $\delta_1=\delta_2=\delta$. Cross-stream integration of (7) for the symmetric wake yields $A-C=\beta(B-D)$ where $\beta\equiv(\int_{-\infty}^{+\infty}f^2d\eta/\int_{-\infty}^{+\infty}f\,d\eta)$. It is shown in Liu *et al.*[15] that for the symmetric wake, B and D are quite small in comparison to A and C. If B and D are neglected, the integral constraint then gives $A\approx C$ and measurements confirm that this is true to good approximation. Similarity then requires $R(x)\sim-\delta d(U_eU_d)/dx\sim U_dd(U_e\delta)/dx$ and $U_d\sim U_e$, where the symbol "~" is to be interpreted as "varies with x in the same manner as." Hence instead of making the *a priori* assumption that the appropriate similarity scaling for the Reynolds stress is U_d^2, we will take $R(x)\sim U_dd(U_e\delta)/dx$. We note that the similarity requirement that $U_d\sim U_e$ would appear to be especially restrictive and, in fact, is only met to good approximation for the APG case [e.g., Figs. 24(b) and 25(b)].

The more general approach to similarity scaling for turbulent free shear flows outlined above was originally suggested by George[23] and was motivated by the observation that wake flows often exhibit a common velocity defect profile but disparate streamwise growth rates that appear related to initial conditions. The observation that wakes possess long memory of initial conditions may be interpreted that multiple self-preserving states exist and are selected based upon initial conditions.

For the asymmetric wake, coefficient E is of the same order as A and C which, in turn, are again larger than B and D. Cross-stream integration of (7) still yields $A\approx C$ since

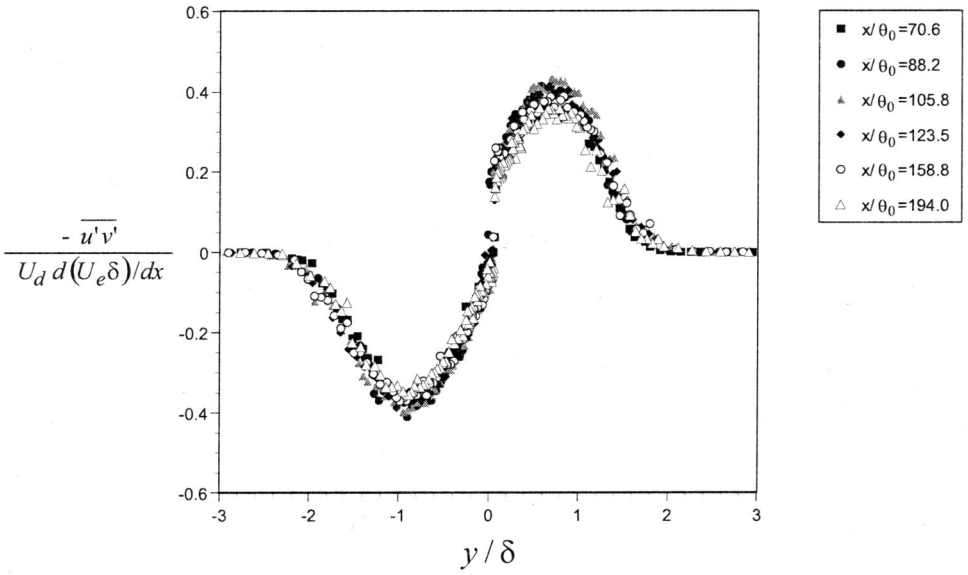

FIG. 22. Scaled symmetric wake Reynolds stress profile for APG case.

$U_e U_d dy_d/dx \int_{-\infty}^{+\infty} f'\, d\eta = 0$. As for the symmetric wake, the Reynolds stress scaling will be $R(x) \sim U_d d(U_e \delta)/dx$ with $\delta = (\delta_1 + \delta_2)/2$. For asymmetric wake similarity we again have the requirement that $U_d \sim U_e$ and we have the additional imposed constraint that $dy_d/dx \sim d\delta_i/dx$. Although not presented here, measurements reported in Liu[14] show that, to good approximation, y_d/δ_1 and y_d/δ_2 are approximately constant although the values of the constant are not the same since the two wake shear layers have disparate growth rates.

Figures 21(a) and 21(b) present cross-stream $-\overline{u'v'}$ profiles measured in the asymmetric wake (by x-wire probe) that span a representative range of streamwise locations for the APG and FPG conditions, respectively. The Reynolds stress has been normalized by $R(x) \equiv U_d d(U_e \delta)/dx$ and the relative lateral coordinate $(y - y_d)$ by δ_i. In both cases the collapse is observed to be surprisingly good (given the fact that the measurements are confined to the near wake) with the Reynolds stresses exhibiting a slightly asymmetric cross-stream shape. The cross-stream asymmetry is consistent with the previously observed slight asymmetry of the scaled wake mean velocity profiles. Note that the collapse is best for the APG case. This is not surprising since only in the APG case is $U_d \sim U_e$ as strictly required for similarity. Despite the collapse, the scaled Reynolds stress profiles are not the same and clearly depend on the applied pressure gradient environment. Similar results were also obtained for the symmetric wake in pressure gradient. An example is presented in Fig. 22 which presents scaled Reynolds stress profiles for the APG case. These symmetric wake data were acquired via LDV and the reason for the relative scarcity of data near $y/\delta = 0$ is due to limitations imposed by seeding.

The apparent success of $R(x) = U_d d(U_e \delta)/dx$ to scale the measured Reynolds stresses suggests scaling cross-stream profiles of the rms streamwise fluctuation $\sqrt{\overline{u'^2}}$ as measured for the asymmetric wake in APG, ZPG, and FPG by the velocity scale $[U_d d(U_e \delta)/dx]^{1/2}$. Figure 23 presents these data. The degree of collapse is observed to be superior to that shown by the corresponding profiles in Fig. 20 using the traditional scaling, $\sqrt{\overline{u'^2}}/U_d$. As before, however, the FPG case exhibits the greatest degree of scatter and the APG case the best collapse.

C. Numerical simulation of the wake in pressure gradient

In order to assess the ability of commonly used turbulence models to capture the global evolution of the symmetric and asymmetric wakes in constant pressure gradient, complementary numerical simulations were performed. These simulations are based on the thin shear layer form of the Reynolds-averaged Navier–Stokes equations for incompressible flow, Eqs. (5) and (6). The use of the thin shear layer form of the governing equations permits the use of a simple, efficient, parabolic marching scheme. The numerical scheme employed is second order accurate in x and y, and is fully implicit with conservative central differencing in the y direction and backward differencing in x. Prior to running the turbulent wake simulations, the numerical scheme was validated against the laminar wake asymptotic series solution of Goldstein[24] and was found to show excellent agreement.

For the symmetric and asymmetric wake simulations the turbulence models utilized were the Spalart–Allmaras one-equation model and the Wilcox $k-\omega$ two-equation model. In implementing theses models the momentum equation is decoupled from the turbulence model transport equations by using velocity values at the nearest upstream nodal points. Standard model constants were used and no attempt was made to optimize the turbulence models for this particular flow. Initial conditions for the computations were the mean velocity profile and the Reynolds stresses at $x = 12.7$ cm (i.e., well upstream of imposition of the pressure gradient). Details regarding the implementation of the numerical scheme may be found in Brooks.[25]

Figures 24(a) and 24(b) present a comparison between measured and computed streamwise variations in wake

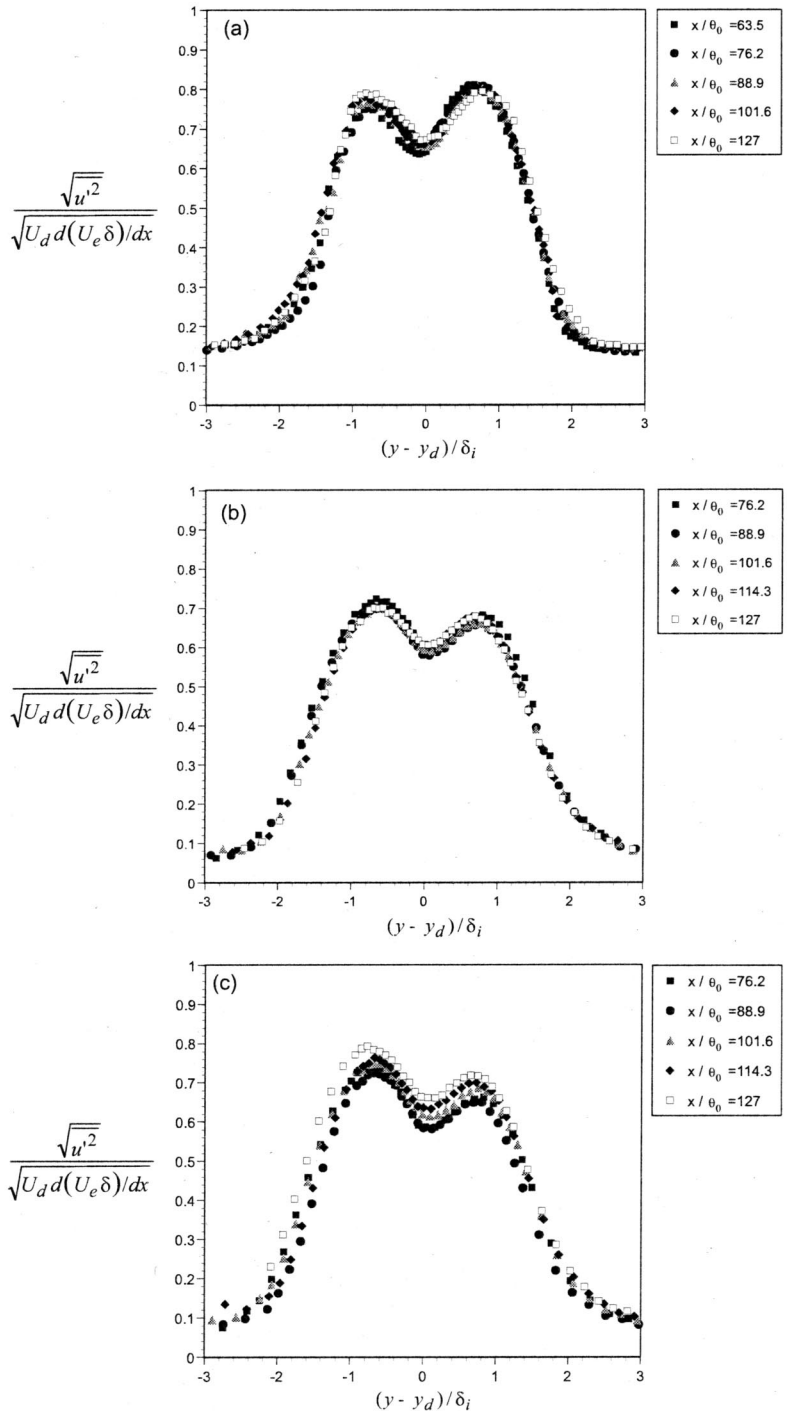

FIG. 23. Cross-stream profiles of $\sqrt{u'^2}/\sqrt{[U_d d(U_e\delta)/dx]}$ for the asymmetric wake in (a) APG; (b) ZPG, and (c) FPG cases.

spreading and mean velocity defect, respectively, for the symmetric wake APG, ZPG, and FPG cases. These figures show that both computations are able to faithfully capture the effect of constant pressure gradient on the streamwise evolution of global wake mean flow parameters. There is little in these figures to motivate the use of the more complicated two-equation model over the simpler one-equation Spalart–Allmaras model.

Figures 25(a) and 25(b) present a similar comparison between measured and computed streamwise variations in wake spreading and maximum velocity defect, respectively, for the asymmetric wake APG and FPG cases. The deviations between experiment and computation are greater than for the symmetric wake in pressure gradient. With regard to the asymmetric wake widening, as shown in Fig. 25(a), the Wilcox $k-\omega$ model accurately captures the wake growth in APG while it is overpredicted by the Spalart–Allmaras model. In FPG, however, the Spalart–Allmaras model does a better job capturing the streamwise variation in wake width, which is underpredicted by the Wilcox $k-\omega$ model. Figure 25(b) shows that both turbulence models do a satisfactory job in capturing the velocity defect variation for the FPG

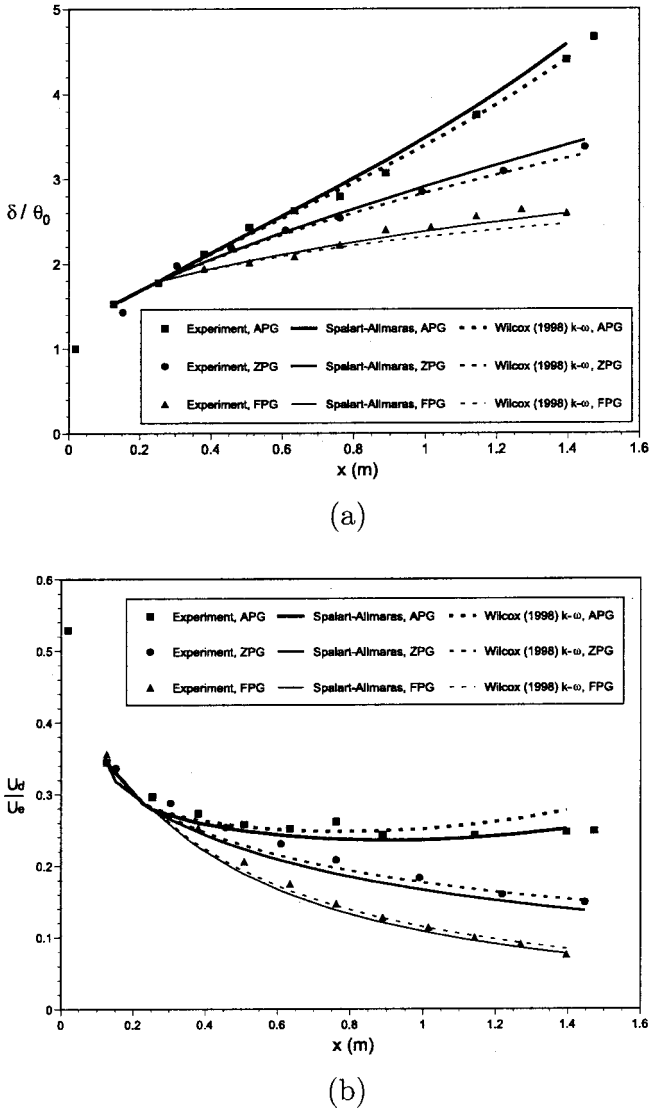

FIG. 24. Comparison of measured and computed streamwise variation in (a) wake spreading and (b) maximum velocity defect for the symmetric wake.

case. For the APG case, however, both underpredict the defect decay rate observed in the experiment.

Figure 26 presents a streamwise sequence of mean velocity profiles resulting from the computation of the asymmetric wake in APG and clearly shows the same lateral migration of the wake maximum velocity defect location $y_d(x)$ toward the thicker side of the wake as was seen in the experiments. Since the pressure gradient is directly imposed in the computations and does not explicitly include the curved diffuser walls, this serves to illustrate that this effect is a generic aspect of the asymmetric wake development and is not attributable to a peculiarity of the flow field facility.

V. CONCLUSION

Due to the disparate boundary layer development that occurs over the top and bottom surface of a high-lift system element, the wake tends to be inherently asymmetric. The asymmetric wake develops in a strong pressure gradient environment and subsequently interacts with downstream elements. In order to isolate the effect of wake asymmetry, a detailed experimental investigation has been performed to characterize both the mean and turbulent flow development of symmetric and asymmetric wakes exposed to identical (constant) pressure gradients. Initial wake asymmetry is achieved by means of both passive and active flow control applied to both sides of a wake-generating plate.

In the absence of imposed streamwise pressure gradient, it is found that the asymmetric wake spreads faster than the corresponding symmetric wake. The spreading rate of the thinner wake shear layer exceeds that of the thick shear layer and consequently, the asymmetric wake mean velocity profile tends to become more symmetric in shape as the wake develops downstream. In contrast, wake asymmetry has no effect on the streamwise variation of the local maximum velocity defect. The center of the asymmetric wake (as defined by the lateral position of the local maximum velocity defect) is found to migrate toward the thicker wake shear layer with increases in x. This effect, which was also observed in complementary asymmetric wake numerical simulations, is found to be a direct consequence of the asymmetry of the Reynolds stress distribution.

The imposed pressure gradients have a profound effect on both the symmetric and asymmetric wake mean flow development. Compared to the zero pressure gradient case, the imposed adverse pressure gradient greatly enhanced the spreading rate for both symmetric and asymmetric wakes. For both the symmetric and asymmetric wakes in FPG, the wake widening is reduced below that for the ZPG case. As was the case for ZPG, however, the asymmetric wake in FPG widens at a greater rate than the corresponding symmetric FPG case. The symmetric and asymmetric wakes in APG exhibit virtually identical streamwise growth with both spreading approximately exponentially with x.

The velocity defect decay rate is reduced by the imposition of the adverse pressure gradient and increased by the favorable pressure gradient. The streamwise variation of the velocity defect exhibits a virtually identical dependence on imposed pressure gradient for corresponding symmetric and asymmetric cases indicating that wake asymmetry has virtually no effect on the defect decay rate.

By scaling the local velocity defect $U_e-\overline{U}$ by $U_d(x)$ and the lateral spatial coordinate y by the mean velocity half-width, $\delta(x)$, symmetric wake mean velocity profiles exhibit similarity and are nearly universal in shape despite the different imposed pressure gradients. In fact, the self-similar symmetric wake profile shape observed for the wake-in-pressure gradient matches that used by Wynganski *et al.*[21] to collapse wake profiles from a variety of wake-generating bodies under ZPG conditions. For the asymmetric wake the defect was scaled with $U_d(x)$ (since wake asymmetry had no effect on the maximum defect) but the lateral coordinate (relative to y_d) was scaled by δ_i, $i=1, 2$, where $\delta_1(x)$ and $\delta_2(x)$ denote the half-widths of the thick and thin wake shear layers, respectively. This scaling was found to yield a nearly symmetric, self-similar profile shape which was largely independent of the applied pressure gradient. For both symmetric and asymmetric wakes, the similarity is incomplete in the

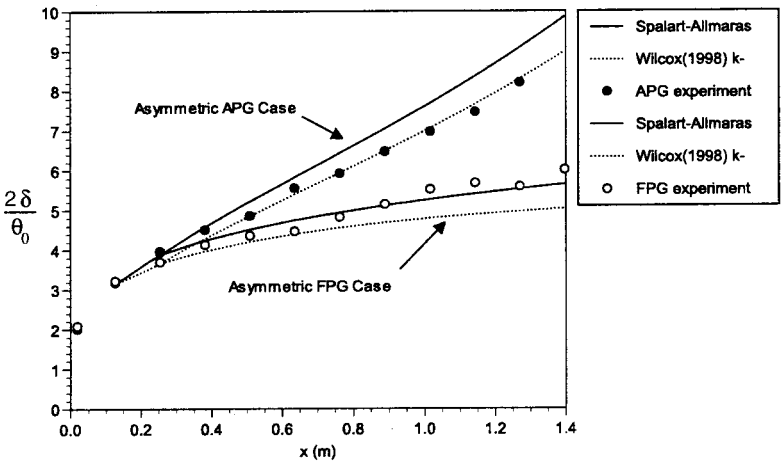

(a)

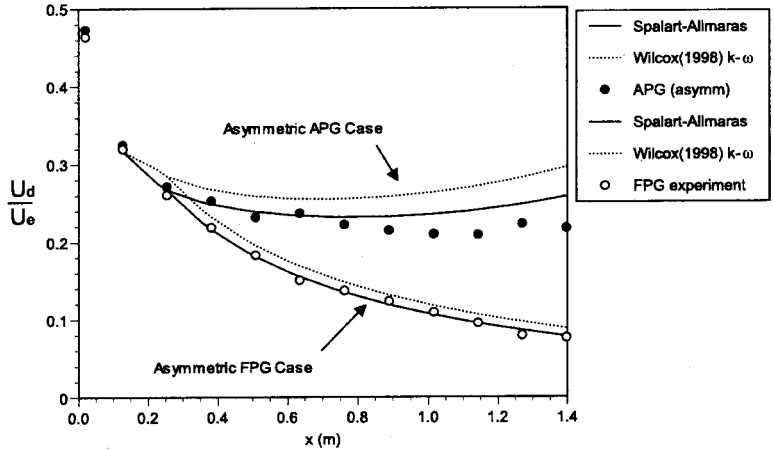

(b)

FIG. 25. Comparison of measured and computed streamwise variation in (a) wake spreading and (b) maximum velocity defect for the asymmetric wake.

sense that second order turbulence statistics generally do not exhibit collapse over the streamwise range covered by the experimental apparatus.

Despite the strong effect of pressure gradient on $U_d(x)$ and $\delta(x)$ individually, for both symmetric and asymmetric wakes the streamwise variation of the quantity U_d/δ_i was found to be independent of the applied pressure gradient. This quantity is intimately related to the local maximum strain rate, $|\partial U/\partial y|_{i,\max}=(U_d/\delta_i)|f'|_{\max}$. Hence the local mean strain rate $\partial U/\partial y$ will be independent of the imposed streamwise pressure gradient. It is, of course, a strong function of the wake asymmetry, however. Recall that the mean spanwise vorticity $\Omega_z \approx -1/2\partial U/\partial y$ is initially identical in each pressure gradient case due to maintenance of the same initial conditions. The Reynolds-averaged vorticity transport equation shows that the redistribution of spanwise vorticity will be independent of the direct effects of the imposed pressure gradient since $\nabla \times \nabla P = 0$.

It was found that for both symmetric and asymmetric wakes, the imposed adverse pressure gradient sustains higher levels of turbulent kinetic energy over larger streamwise distances than does the corresponding zero pressure gradient wake. In contrast, the favorable pressure gradient case exhibits a more rapid streamwise decay of the turbulent kinetic energy relative to the zero pressure gradient case. For asymmetric wakes, the turbulent kinetic energy profiles are initially asymmetric but approach a symmetric shape as they evolve in x. The approach to symmetry is most rapid for the APG case and slowest for the FPG.

Despite the imposed streamwise pressure gradients, comparison of local turbulent shear and dilatational production mechanisms revealed that the wake was shear dominated. For the asymmetric wake, the higher turbulence production rates in the thin wake shear layer (associated with higher $\partial U/\partial y$) is, in large part, responsible for the turbulent kinetic energy profiles approaching cross-stream symmetry as shown in Fig. 14. Explanation of the pressure gradient-dependent differences in the evolution of the turbulent field requires the dilatational production mechanism to play a key role. It is found that even though the wake is shear dominated, pressure gradient-dependent differences in the local Reynolds stress have their origin in dilatational terms. Once created, these disparities in Reynolds stress give rise to significant differences in shear turbulence production that are

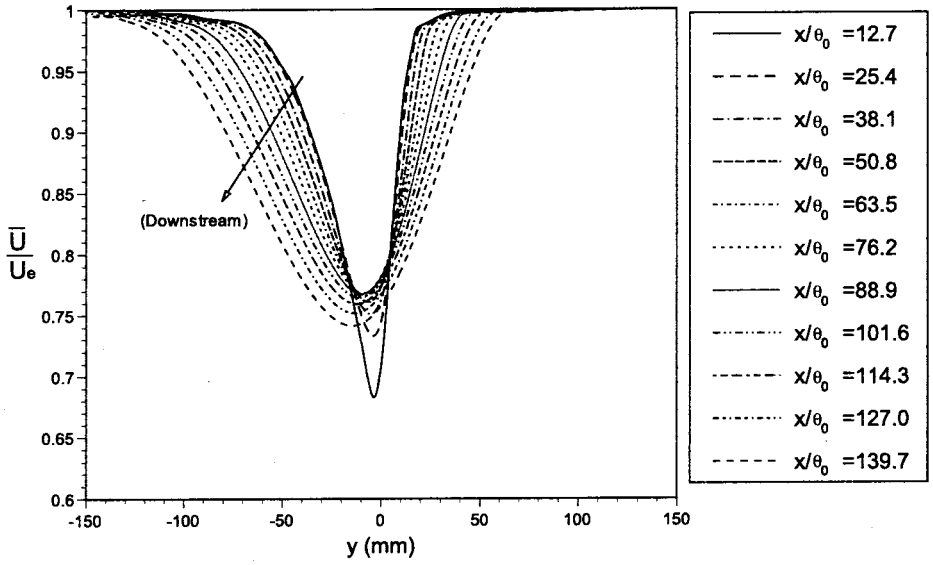

FIG. 26. Computed streamwise sequence of mean velocity profiles of the asymmetric wake under APG condition based on the Spalart–Allmaras model.

largely responsible for the observed effect of pressure gradient on the turbulent kinetic energy. In support of this, it is found that the difference in local turbulence production between the APG and FPG cases is primarily associated with dilatational mechanisms just downstream of x_p while the shear term dominates farther downstream.

Profiles of $-\overline{u'v'}/k$ for both the asymmetric and symmetric wakes exhibited collapse under FPG, ZPG, and APG conditions. That $-\overline{u'v'}$ scales with k is equivalent to stating that the b_{uv} component of the anisotropy tensor is nearly invariant with respect to streamwise coordinate. Hence the neglect of variations in $-\overline{u'v'}$ that are due to the anisotropy tensor while retaining those due to k is a very reasonable approximation for the strained turbulent wake flow. This indicates that the ''weak-equilibrium assumption'' proposed by Rodi which is inherent to algebraic Reynolds stress closure models is entirely appropriate for this class of flows.

Scaling the Reynolds stress profiles in the traditional manner by U_d^2 fails to produce collapse. Examination of the transformed governing equation (7) suggests that the appropriate scaling for the Reynolds stress is $R(x) = U_d d(U_e \delta)/dx$. Indeed, when scaled in this fashion, both the asymmetric and symmetric wake Reynolds stress profiles exhibit an impressive collapse for FPG, ZPG, and APG cases. This was the case despite the fact that the experiments are focused on near-wake development. The degree of collapse is generally best for the APG case and worst for the FPG case. This may be due, in part, to the APG case most closely satisfying the mean flow similarity requirement that $U_d \sim U_e$. Despite the collapse, the scaled Reynolds stress profiles are different for each pressure gradient case. Although similarity at the level of the normal stress transport equation was not considered, scaling profiles of $\sqrt{\overline{u'^2}}$ by $\sqrt{U_d d(U_e \delta)/dx}$ produced a better degree of collapse than did the traditional scaling by U_d. Again, the APG case exhibited the best collapse. One gets the impression from the experimental results that the APG case accelerates the development of the turbulent field while the FPG condition retards it.

Complementary numerical simulations of the symmetric and asymmetric wake in pressure gradient were performed. For the symmetric wake, both the Spalart–Allmaras and the Wilcox $k-\omega$ turbulence models are able to faithfully capture the effect of constant pressure gradient on the streamwise evolution of global wake mean flow parameters. For the asymmetric wake simulations, the agreement between computations and experiment is not as good. The Wilcox $k-\omega$ model captures the wake spreading in the APG case. It is overpredicted by the Spalart–Allmaras model. For the FPG case, the Spalart–Allmaras model captures the wake spreading which is underpredicted by the two-equation model. Both models underestimate the defect decay rate for the APG case but capture it quite faithfully for the FPG case.

ACKNOWLEDGMENTS

This research was supported by NASA Langley Research Center, Hampton, VA, under Grant No. NASA NAGI-1987, monitored by Ben Anders. This support is gratefully acknowledged.

[1] P. L. Garner, P. T. Meredith, and R. C. Stoner, ''Areas for CFD development as illustrated by transport aircraft applications,'' AIAA Pap. 91–1527 (1991).
[2] A. M. O. Smith, ''High-lift aerodynamics,'' AIAA J. Aircraft **12**, 501 (1975).
[3] D. M. Driver and G. M. Mateer, ''Wake flow in adverse pressure gradient,'' *SAE/AIAA World Aviation Congress and Exposition, San Diego, CA*, SAE Technical Paper 2000-01-5511.
[4] M. J. Tummers, D. M. Passchier, and R. A. W. M. Henkes, ''Experimental investigation of an adverse pressure gradient wake and comparison with calculations,'' Exp. Therm. Fluid Sci. **14**, 17 (1997).
[5] R. Hoffenberg, J. P. Sullivan, and S. P. Schneider, ''Wake measurements in a strong adverse pressure gradient,'' AIAA Pap. 95–1912 (1995).
[6] R. Hoffenberg and J. P. Sullivan, ''Measurement and simulation of a decelerated wake,'' AIAA Pap. 98–0522 (1998).
[7] R. Narasimha and A. Prabhu, ''Equilibrium and relaxation in turbulent wakes,'' J. Fluid Mech. **54**, 1 (1972).

[8]A. Prabhu and R. Narasimha, ''Turbulent non-equilibrium wakes,'' J. Fluid Mech. **54**, 19 (1972).
[9]A. J. Reynolds, ''Observation on distorted turbulent wakes,'' J. Fluid Mech. **13**, 333 (1962).
[10]J. F. Keffer, ''The uniform distortion of a turbulent wake,'' J. Fluid Mech. **22**, 135 (1965).
[11]I. S. Gartshore, ''Two-dimensional turbulent wakes,'' J. Fluid Mech. **30**, 547 (1967).
[12]A. Nakayama, ''Curvature and pressure-gradient effects on a small-defect wake,'' J. Fluid Mech. **175**, 215 (1987).
[13]M. M. Rogers, ''The evolution of strained turbulent plane wakes,'' J. Fluid Mech. **463**, 53 (2002).
[14]X. Liu, ''A study of wake development and structure in constant pressure gradient,'' Ph.D. dissertation, University of Notre Dame, 2001.
[15]X. Liu, F. O. Thomas, and R. C. Nelson, ''An experimental investigation of the planar turbulent wake in constant pressure gradient,'' Phys. Fluids **14**, 2817 (2002).
[16]F. O. Thomas, R. C. Nelson, and X. Liu, ''Experimental investigation of the confluent boundary layer of a high-lift system,'' AIAA J. **36**, 978 (2000).
[17]C. Hah and B. Lakshminarayana, ''Measurement and prediction of mean velocity and turbulence structure in the near wake of an airfoil,'' J. Fluid Mech. **115**, 251 (1982).
[18]S. Acharya, D. Adair, and J. H. Whitelaw, ''Flow over a trailing flap and its asymmetric wake,'' AIAA J. **25**, 897 (1987).
[19]F. W. Roos, ''Experimental studies of wake retardation in a simulated high-lift system flow field,'' AIAA Pap. 97–1813 (1997).
[20]H. Schlichting, *Boundary Layer Theory*, 7th ed. (McGraw-Hill, New York, 1979).
[21]I. Wygnanski, F. Champagne, and B. Marasli, ''On the large-scale structure in two-dimensional, small-deficit, turbulent wakes,'' J. Fluid Mech. **168**, 31 (1986).
[22]S. B. Pope, *Turbulent Flows* (Cambridge University Press, Cambridge, England, 2000).
[23]W. K. George, ''The self-preservation of turbulent flows and its relation to initial conditions and coherent structures,'' in *Advances in Turbulence*, edited by W. K. George and R. E. A. Arndt (Hemisphere, New York, 1989), pp. 39–73.
[24]S. Goldstein, ''Concerning some solutions of boundary layer equations in hydrodynamics,'' Proc. Cambridge Philos. Soc. **XXVI**, 1 (1929).
[25]G. Brooks, ''Numerical simulation of a planar turbulent wake in arbitrary pressure gradient,'' M.S. thesis, University of Notre Dame, 1999.